M 2021

U.PORTO
FEUP FACULDADE DE ENGENHARIA
UNIVERSIDADE DO PORTO

ELECTROCHEMICAL CONVERSION OF CO_2 INTO HYDROCARBONS

MARIANA ALMEIDA BAPTISTA
DISSERTAÇÃO DE MESTRADO APRESENTADA
À FACULDADE DE ENGENHARIA DA UNIVERSIDADE DO PORTO EM
CHEMICAL ENGINEERING

Master in Chemical Engineering

Electrochemical conversion of CO_2 into hydrocarbons

Master dissertation

of

Mariana Almeida Baptista

Developed within the course of dissertation

held in

DMT Environmental Technology / R&D department



Supervisor at FEUP: **Dr. Ana Mafalda Ribeiro**

Coordinator at DMT : **Msc. Jort Langerak**





July 2021

Acknowledgment

I want to start by thanking DMT Environmental Technology for given me the opportunity to develop my master thesis on such an interesting subject, for all the knowledge transmitted, and for the job experience. I have to say that I grow so much in the last months and I am glad for the amazing experience that I had. This internship has given me the certainty of the direction and contribution I intend to make in the future as a chemical engineer.

I would like to give a special thanks to the supervisor at FEUP, Ana Mafalda Ribeiro, as well as to Maria Marcela Fragozo for the availability to meet with me and answer my questions whenever necessary. Also, a particular thanks to my supervisor at DMT, Jort Langerak, to Benny Bakker, and all the people at DMT that had somehow impact my journey, for welcoming me, and made an effort to make me feel integrated.

I am thankful to all the amazing friends that I made and with whom I had the pleasure to share my academic journey. A special thanks to Luísa for being there since the beginning and for the company. To the girls I have shared these past few months with, Alexandra, Carina, Francisca, Melanie, and, Tânia, thank you for all the moments we had while living together and for exploring the Netherlands with me.

Finally, I am beyond grateful to my parents, my sister, and all my closest family, for all the love, the endless support, and for always being present during my entire life.

Professor Ana Mafalda Ribeiro, supervisor of this dissertation, is member of the Associate Laboratory LSRE-LCM funded by national funds through FCT/MCTES (PIDDAC): Base Funding UIDB/50020/2020.





Abstract

The rising levels of CO_2 in the atmosphere contribute to climate degradation and global warming. This problem must be overcome by the introduction and promotion of more sustainable energy sources at competitive prices, low and negative carbon technologies, and decarbonization technologies. As an example, the electrochemical reduction of CO_2 to chemicals (e.g., oxalic acid) allows to sustainably close the carbon cycle while generating valuable products.

Oxalic acid has several industrial applications and is currently being produced by different routes, but all of them emit CO_2. So in comparison, its production through electrochemical CO_2 reduction (ECR) would be advantageous and would allow valuing a waste stream that is being produced by Carborex®MS which may allow DMT to enter in emerging markets. Moreover, comparing with other chemicals production, oxalic acid seems to be the simplest C_{2+} product to produce, requiring the lowest energy input. Therefore, this thesis was focused on the study of the electrochemical conversion of CO_2 to oxalic acid.

Until now, this topic has not been studied in great depth and there is no industrial application yet. Thus, a first global research on how ECR processes are affected was carried out to understand the main variables and challenges, such as electrolyte, pressure, temperature, pH, feedstock, separators, electrolyzer configuration, and electrocatalyst. Based on that, two different systems for specific oxalic acid production were considered and evaluated with regard to process design (considering two different situations where CO_2 would be directly fed to the cell as a gas or dissolved in the electrolyte), mass and energy balances over the global process and the electrolyzer, and its economic feasibility was also carried out. It was concluded that Approach 2 would be the best system option. However, a lot of assumptions and simplifications were made and a deeper analysis of the entire system (considering upstream processes, the reactor, and downstream processes) would be recommended for a more meaningful analysis. Additionally, a parametric analysis was carried out as a way to study the behaviour of some kinetic parameters for the systems considered.

Keywords: Electrochemical CO_2 reduction; Oxalic acid;

Resumo

Nos últimos anos, os níveis de CO_2 na atmosfera têm aumentado consideravelmente, o que contribui para a degradação climática e o aquecimento global. De forma a ultrapassar este problema, é necessário introduzir e promover fontes energéticas mais sustentáveis (e a preços competitivos), tecnologias com um impacto carbónico baixo ou negativo, assim como, technologias que permitam a descarbonização da industria. Como exemplo, a redução eletroquímica do CO_2 permite fechar o ciclo de forma sustentável e produzir compostos químicos com valor acrescentado (ex., ácido oxálico).

O ácido oxálico têm várias aplicações industriais e pode ser produzido por diferentes processos. Contudo, todos os processos atualmente usados emitem CO_2. Desta forma, e em comparação com os processos atuais, a produção de ácido oxálico através da redução eletroquímica do CO_2 seria vantajoso e permitiria à DMT usar a corrente rica em CO_2 produzida pela Carborex®MS que, de outra forma, seria desperdiçada. Adicionalmente, em comparação com outros compostos, o ácido oxálico aparenta ser o composto com dois carbonos mais simples de produzir que necessita da menor quantidade energética. Desta forma, esta tese focou-se no estudo da conversão eletroquímica do CO_2 em ácido oxálico.

Até à data, este tópico não tem sido muito estudado e ainda não existe nenhuma aplicação industrial para esta produção específica. Assim sendo, foi feita uma pesquisa geral dos principais parâmetros e obstáculos do processo, tais como, o tipo de eletrólito usado, pressão, temperatura, pH, alimentação, os tipos de separadores, as configuração da célula e os catalisadores. Partindo dessa pesquisa, dois sistemas diferentes para a produção especifica do ácido oxálico foram escolhido e avaliados (considerando a alimentação direta do CO_2 na célula como um gás ou dissolvido no eletrólito) através da realização de balanços de massa e energéticos ao sistema global, assim como ao eletrolizador, e averiguando a viabilidade económica de cada sistema. Concluiu-se que a Abordagem 2 seria a melhor opção. Contudo, muitas suposições e simplificações foram feitas ao longo do trabalho pelo que, uma análise mais profunda de todo o sistema (considerando os processos a montante, o reator e os processos a jusante) seria recomendada para validar as conclusões retiradas. Adicionalmente, foi realizada uma análise paramétrica para avaliar o comportamento de alguns parâmetros cinéticos dos sistemas considerados.

Palavras-chave: Redução eletroquímica do CO_2; Ácido oxálico;

Declaration

I hereby declare, under word of honour, that this work is original and that all non-original contributions is indicated and due reference is given to the author and source

Mariana Almeida Baptista

5th July 2021

Index

1 Introduction 1
1.1 Framing and presentation of the work 1
1.2 Presentation of the company 2
1.3 Contribution of the author to the work 3
1.4 Organization of the dissertation 3
2 Context and State of the art 5
2.1 Current routes for $\mathbf{CO_2}$ reduction to CO 5
2.1.2 Oxalic acid 7
2.2 ECR process variables 8
2.3 House of quality 15
3 Materials and Methods 17
3.1 ECR systems considered 17
3.2 Mass and energy balances 19
3.3 Parametric analysis 21
3.5 Business case 24
4 Results and discussion 25
4.1 Mass and energy balances 25
4.2 Parametric analysis 32
4.3 Business case 36
5 Conclusions 41
6 Assessment of the work done 43
6.1 Objectives Achieved 43
6.2 Final Assessment 43
7 References 45
Appendix A - Electrolyzer configurations 49
Appendix B - House of Quality 51
Appendix C - Parametric analysis graphs' data 53
Appendix D - Storage tanks costs 55

List of Figures

Figure 1- Energy consumption (TWh) by source and average global atmospheric CO_2 concentration (ppm) from 1800 to 2019. Adapted from [1, 4]. 1

Figure 2- Pourbaix diagram for carbon at 25 °C considering predominate gaseous species (italic) and solution phase species as well as (a) lower stability window of water (HER) and (b) upper stability limit of water (O_2 evolution reaction (OER)) [36]. 11

Figure 3- Different types of ion exchange membranes (IEM): a) CEM, b) AEM, and c) BPM. The letters A and C stand for anode and cathode, respectively. Adapted from [39]. 12

Figure 4- Schematic representation of a) conventional H-cell reactor; b) two chambers liquid-fed electrolyzer; c)- vapor-fed electrolyzer; and d) microfluidic reactor. The numbers stand for: (1) cathode, (2) anode, (3) separator, (4) anolyte, and (5) catholyte. Adapted from [10, 38] 14

Figure 5- Typical polarization curve as a function of current density, showing the dependent regimes controlled by the activation, concentration, and ohmic overpotentials. Adapted from [70]. 23

Figure 6- PFD for Approach 1-a) and b), and Approach 2-a) and b). 25

Figure 7- Schematic representation of the cells for Approach1-a) and b), and Approach 2-a) and b). 28

Figure 8- Parametric analysis of ηact as a function of i when $i_0 = 1.00\ A{\cdot}m^{-2}$ and $1.71 \times 10^{-4}\ A{\cdot}m^{-2}$ and $\alpha_A = 0.021$, 0.100 and 0.258 for Approach 1. 33

Figure 9- Parametric analysis of ηact as a function of i when $i_0 = 1.00\ A{\cdot}m^{-2}$ and $1.71 \times 10^{-4}\ A{\cdot}m^{-2}$ and $\alpha_A = 0.023$, 0.100 and 0.282 for Approach 2. 33

Figure 10- Parametric analysis of ηact as a function of i when $i_{0,Pb} = 2.50 \times 10^{-9}\ A{\cdot}m^{-2}$ and $i_{0,Zn} = 3.00 \times 10^{-7}\ A{\cdot}m^{-2}$ and $\alpha_A = 0.021$, 0.100 and 0.258 for Approach 1. 34

Figure 11- Parametric analysis of ηact as a function of i when $i_{0,Pb} = 2.50 \times 10^{-9}\ A{\cdot}m^{-2}$ and $i_{0,Pt} = 5.00\ A{\cdot}m^{-2}$ and $\alpha_A = 0.023$, 0.100 and 0.282 for Approach 2. 34

Figure 12- Comparison of the values of ηact for Approach 1 and 2, respectively. 35

List of Tables

Table 1- Standard potential for ECR in aqueous media at 25 °C and 1 atm [15]. 6

Table 2- Physical properties of anhydrous oxalic acid [18, 21]. 7

Table 3- Main products obtained with different metal electrocatalysts in both aqueous and non-aqueous electrolyte solutions [9, 15]. 14

Table 4- η_{FE} and products obtain using selective electrocatalysts to oxalic acid production at 2.8 V vs. Ag/AgCl/(0.01 M LiCl + 0.1 M TEAP)/PC in 0.1 M TEAP/PC, and at 100 C [35]. 15

Table 5- Electrolytes parameters. 16

Table 6- Composition of the CO_2-rich feed stream of DMT's Carborex®MS. 19

Table 7- Streams table for Approach 1- a). 26

Table 8- Streams table for Approach 1- b). 26

Table 9- Streams table for Approach 2-a). 27

Table 10- Streams table for Approach 2-b). 27

Table 11- Mass balances ($kg \cdot h^{-1}$) to components within the electrolytic cell for Approach 1- a). 29

Table 12- Mass balances ($kg \cdot h^{-1}$) to components within the electrolytic cell for Approach 1- b). 29

Table 13- Mass balances ($kg \cdot h^{-1}$) to components within the electrolytic cell for Approach 2- a). 30

Table 14- Mass balances ($kg \cdot h^{-1}$) to components within the electrolytic cell for Approach 2- b). 30

Table 15- Energy considerations of Approach 1 and 2. 31

Table 16- Parameters considered and calculated for both Approaches 1-a) and b), and Approach 2-a) and b). ... 32

Table 17- Volumes requided to be stored and corresponding tanks considered. 37

Table 18- Prices of the raw materials, utilities, catalyst, and products considered for the business case. 38

Table 19- Cost analysis for Approach 1-a) and b) and Approach 2-a) and b). 39

Table A 1- Summary of main advantages and disadvantages of the possible ECR electrolyzer configurations. Adapted from [11, 10, 14, 35, 36]. 49

Table A 2- "House of Quality". 51

Table A 3- Dimension properties and costs of the tanks considered. 55

Notation and Glossary

Variables

S	Allowable stress	Pa
q	Amount of charge supplied to the system	C
E_A/E_C	Anode/cathode potential	V
A	Area	m^2
I_{base}	Base cost index	€
E	Cell potential	V
l	Conducting length	m
C	Corrosion allowance	m
I	Cost index	€
C_{PL}	Cost of the platforms and ladders	€
C_P	Cost of the purchase	€
C_V	Cost of the vessel	€
A_0	Cross-section area	m^2
I	Current	A
i	Current density	$A \cdot m^{-2}$
EPC	Electric power consumption	$Wh \cdot kg^{-1}$
F	Faraday's constant	$A \cdot s \cdot mol^{-1}$
i_0	Global exchange current density	$A \cdot m^{-2}$
H	Height	m
D_i	Internal diameter	m
r_i	Internal radio	m
k_f/k_b	Kinetic reaction constants of the forward/backward reaction	$m \cdot s^{-1}$
i_L	Limiting current density	$A \cdot m^{-2}$
F_M	Material factor	-
$[Red]/[Ox]$	Molar concentration of the reduced/oxidized species	$mol \cdot m^{-2}$
n	Moles of electrons transferred per mole of product	$mol \cdot mol^{-1}$
z	Number of moles of product formed	mol
R_o	Ohmic resistance	Ω
Δt	Operational time	s
P	Pressure	Pa
c	Product mass flow	$kg \cdot s^{-1}$
Qr	Reaction quotient	-
c_p	Specific heat	$kJ \cdot kg^{-1} \cdot K^{-1}$
j_f/j_b	Surface reaction speed	$mol \cdot m^{-2} \cdot s^{-1}$
T	Temperature	K
$T_{increase}$	Temperature increase	K
Q	Thermal flow	W
f	Total flow in or out the electrolyzer	$kg \cdot s^{-1}$
R	Universal gas constant	$J \cdot K^{-1} \cdot mol^{-1}$
t	Wall thickness	m
W	Weight	kg
E	Weld efficiency fraction	-

Greek letters

$\eta_{act,A}/\eta_{act,C}$	Anode/cathode activation overpotentials	V
η_{act}	Activation overpotential	V
α_A/α_C	Charge transfer coefficients for anode/cathode	-

η_c	Concentration overpotential	V
κ	Conductivity	$S \cdot m^{-1}$
η_{FE}	Faraday efficiency	%
ρ	Mass density	$kg \cdot m^{-3}$
η_{MM}	Molar mass of the final product	$kg \cdot mol^{-1}$
η_o	Ohmic overpotential	V
η	Overpotential	V

List of Acronyms

AcN	Acetonitrile
AEM	Anion exchange membranes
BM	Bipolar membranes
CAPEX	Capital expenditures
CCS	Carbon capture and storage
CCU	Carbon capture and utilization
CEM	Cation exchange membranes
DESs	Deep eutectic solvents
DEMS	Differential electrochemistry mass spectrometry cells
ECR	Electrochemical CO_2 reduction
GDE	Gas diffusion electrode
GHG	Greenhouse gas
HER	H_2 evolution reaction
IEM	Ion exchange membranes
ILs	Ionic liquids
LCA	Life Cycle Analysis
MEA	Membrane electrode assembly
MFC	Microfluidic flow cell
OPEX	Operational expenses
PEM	Polymer electrolyte membrane cells
PFD	Process flow diagrams
PC	Propylene carbonate
ROI	Return on investment
RWGS	Reverse water gas-shift reaction
SOEC	Solid-oxide electrolysis cell reactor
SHE	Standard hydrogen electrode
TEA	Techno-Economic Analysis
TRL	Technology readiness level
TBAP	Tetrabutylammonium perchlorate
TEACl	Tetraethylammonium chloride
TCO	Total cost of ownership
[EMIM][BF4]	1-Ethyl-3-methylimidazolium tetrafluoroborate

1 Introduction

1.1 Framing and presentation of the work

Fossil fuels have been widely used as energy sources due to their general availability, low costs, and since most of the technologies and processes implemented nowadays largely depend on them. However, since the industrial revolution, its consumption has increased appreciably (Figure 1). In 2019, fossil fuels provided about 84.3 % of global energy (33.1 % from oil, 27.0 % from coal and 24.2 % from gas), followed by hydropower (6.4 %), nuclear (4.3 %), wind (2.2 %), solar (1.1 %), other renewable energy sources (including geothermal, biomass, wave and tidal, 1.0 %), and biofuels (0.7 %) [1]. The high demand for fossil fuels may affect fuel reserves, causing them to run out sooner than expected but, as the most shocking consequence, fossil fuel burning contribute to the increasing greenhouse gas (GHG) emissions, mainly carbon dioxide (CO_2) which contributes to climate degradation, global climate change, and global warming [2] (Figure 1). This highlights the need to revolutionize and rethink the current energy model, allowing the introduction of more sustainable energy sources at competitive prices, low and negative carbon technologies, and decarbonization technologies, as set out within long-term targets for climate change mitigation in Paris Climate Agreement [3].

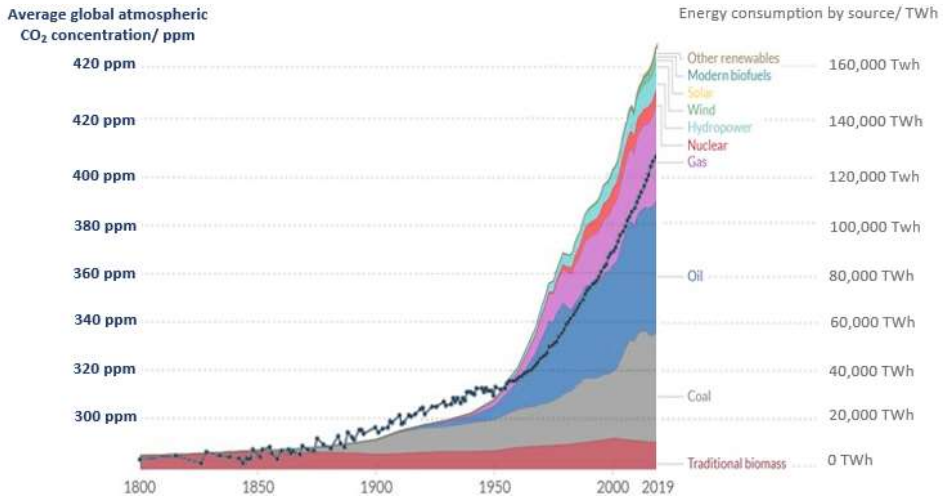


Figure 1- Energy consumption (TWh) by source and average global atmospheric CO_2 concentration (ppm) from 1800 to 2019. Adapted from [1, 4].

Several strategies to reduce CO_2 concentration in the atmosphere have been proposed. Carbon capture and storage (CCS) focus on CO_2 removal, compression, transportation, and storage in deep underground formations (e.g., depleted oil and gas fields, deep saline formations, aquifers, or mineral storage) for long periods to avoid its emission to the atmosphere. Carbon Capture and Utilization (CCU) goes beyond CCS to directly use or convert captured CO_2 into valuable products such as renewable fuels and chemicals (e.g., oxalic acid) as well as use it as an energy storage vector. Thus, the carbon cycle is sustainably closed [4], while valuing one of the largest waste streams feedstocks [5], promoting the decarbonization/defossilization

of the chemical industry and a neutral CO_2 economy, and avoiding the risks of sequestration and geological leakage of long-term CO_2 [6].

After an initial overview of the current routes for CO_2 reduction to carbon monoxide (CO), electrochemical CO_2 reduction (ECR) was pointed as having great potential for the selective production of a wide range of value-added chemicals, namely multi-carbons hydrocarbons, acids or alcohols, which are more desirable due to their higher energy density, and wider applicability. Hence, a clear understanding of the main constraints and principles behind ECR is required for raising its technology readiness level (TRL) and market penetration. The scope of this work will focus on the study of oxalic acid production through an ECR process while addressing all the variables intrinsic to the process as well as its feasibility and economic potential.

1.2 Presentation of the company

DMT Environmental Technology is an engineering company from the Netherlands with a worldwide presence focused on the development and provisioning of efficient environmental technologies contributing in this way to a "clear and prosperous future". To date, the core business model adopted by DMT has been focused on three main areas: biogas upgrading (Carborex), water treatment (TurboTec), and gas desulphurization (Sulfurex). Outside these areas of focus, DMT continuously explores other relevant, innovative ideas and opportunities in emerging green technology markets by working closely with different companies, universities, and students from around the world. In the last few months, DMT has been enrolled in a consertium with VoltaChem, Mestverwerking Fryslan, Tielo-Tech, TNO, and TU Delft for a two-year project called Bio-cel (nr. TEE 119012) [5]. The consortium has received a 352,500 € grant amount to develop an integrated process for the capture and electrochemical conversion of biogenic CO_2 (e.g., obtain from biogas upgrading) to oxalic acid. The key activities of the project consist of (1) screening of solvent-electrolyte combinations, (2) experimental optimization of the combined CO_2 capture, conversion step, and product recovery step, and (3) process design and scale-up based on a Techno-Economic Analysis (TEA) and Life Cycle Analysis (LCA), the latter is DMT responsibility. The industrial implementation and commercialization of electrochemical conversion of CO_2 into oxalic acid will contribute to CO_2 mitigation since the proposed process approximately consumes 2 kg of CO_2 per kg oxalic acid produced. Besides, it allows the decentralization of fossil fuel dependency for the chemical synthesis of other high-value products. From DMT's point of view, the success of this project is particularly relevant, as it could allow its entry into new markets and attract new customers who may be interested in using CO_2-rich feed streams produced by Carborex®MS.

1.3 Contribution of the author to the work

Despite the increasing interest in electrochemical processes in the past couple of decades, the research delivered so far has been mainly focused on mechanistic aspects, process conditions optimization, and electrocatalyst optimization (as to the morphology and composition). Additionally, ECR implementation at an industrial/commercial scale is currently in the early stage, and, unfortunately, just a few papers have been published regarding the specific production of oxalic acid through an ECR process.

The work that I developed during this internship meets DMT's interest in increasing their knowledge of electrochemistry to make a meaningful contribution to the Bio-cel project (regarding oxalic acid-specific production). Besides and as previously mentioned, it proposes an extra pathway for the valorization of the CO_2-rich feed stream produced by Carborex®MS and stands as a starting point, which may allow entering emerging markets for electrochemical CO_2 valorization. This not only required me to do a global research review on ECR processes, but also on the main challenges, relevant figures of merit, as well as an economic feasibility evaluation.

1.4 Organization of the dissertation

Hereinafter, a brief presentation will be given on how this thesis was organized and what will be included in each of the chapters considered.

- **Chapter 2- Context and State of the art:** contextualization of the project and the work done, the different possible CO_2 reduction pathways, and the main variables and challenges regarding the electrochemical reduction of CO_2. Moreover, a "House of quality" study on electrodes and electrolytes is presented.
- **Chapter 3- Materials and Methods:** presentation of the two systems for ECR considered, the methodology and the tools adopted throughout the project, as well as the assumptions that were held;
- **Chapter 4- Results and discussion:** presentation of the results obtained for the considered systems regarding the mass balances, process flow diagrams (PFD), parametric analysis, and business case that were carried out;
- **Chapter 5- Conclusion:** framing and presentation of the results obtained, as well as the main outputs suggested by the results;
- **Chapter 6- Assessment of the work done:** an overall reflection of the work carried out was done according to the initial goals, future work, main challenges, and recommendations.

2 Context and State of the art

2.1 Current routes for CO_2 reduction to CO

In order to decrease CO_2 concentration in the atmosphere, different CCU pathways are currently used/have been proposed to produce fuels and chemicals. CO_2 can be reduced to CO, through different routes such as photochemical, photoelectrochemical (photocatalysis) or electrochemical reduction, as well as gas and liquid-phase reactions. Each of these routes will be briefly described below. CO is usually highlighted since it is a feedstock for many processes (large market).

Photochemical reduction aims to mimic Nature (photosynthesis process) and reduce atmospheric CO_2 using sunlight as the only energy input and water as source of electrons (water electrolysis- Eq. (1)). For the process to happen, first a molecular photosensitizer absorbs photons and forms a reactive excited state capable of reducing CO_2 through charge transfer. To close the catalytic cycle, the oxidized photosensitizer receives an electron to regenerate the initial molecule. The photosensitizer can be used just to capture incident light (in this case, energy is transferred to a separate cocatalyst or electron mediator where CO_2 reduction happens) or, in addition, can also be used as a catalyst itself [7].

$$2\,H_2O \rightarrow O_2 + 2\,H_2,\ \ \Delta H_{298\,K} = 571.66\ \text{kJ}\cdot\text{mol}^{-1} \qquad \text{Eq. (1)}$$

Photocatalysis reaction takes place in both liquid or gas phase medium at ambient temperature and pressure. The difference between electrochemical reduction and photocatalysis is the source of electrons, which are supplied by exposing a photocatalyst (semiconductor) to light of the desired wavelength. Firstly, electrons absorb photons energy, excite from a valence band to a conduction band and, consequently, a hole is generated in the valence band. In this photoexcitation state, the excited electron is used to reduce an acceptor (reduction of the adsorbed CO_2 molecule to different products), while the hole is used for the oxidation of donor molecules (water electrolysis) [9, 10].

Reverse water gas-shift reaction (RWGS) (Eq. (2)) takes place in both liquid or gas phase medium, uses CO_2 and hydrogen (H_2) to produce CO and water (H_2O) over Cu and novel metal (Pt, Pd, Rh)-based catalyst at temperatures between 200-600 °C [10]. The need for a stream of H_2 is considered as a disadvantage since it is mainly produced from natural gas (48 %), petroleum (30 %), and coal (18 %) through different energy-intensive and environmentally unfriendly methods such as steam reforming, dry-reforming, partial oxidation, and coal gasification (releasing ca. 830 $Mt_{CO2}\cdot yr^{-1}$) [11]. H_2 can be obtained by a more sustainable way through water electrolysis. However, this method only accounts for 4 % of H_2 global production due to the high energy consumption and costs associated [12, 13], .

$$CO_2 + H_2 \rightarrow\ CO\ +\ H_2O,\ \ \Delta H_{298\,K} = 41.16\ \text{kJ}\cdot\text{mol}^{-1} \qquad \text{Eq. (2)}$$

Reverse Boudouard reaction (Eq. (3)), also known as carbon dioxide-char gasification reactions, allow the complete conversion of CO_2 and a solid carbon source to CO. However, the process requires high temperatures (600-900 ℃) [13].

$$CO_2 + C\,(s) \leftrightarrow 2\,CO,\ \ \Delta H_{298\,K} = 172.44\ \text{kJ} \cdot \text{mol}^{-1} \qquad \text{Eq. (3)}$$

Dry reforming of methane (Eq. (4)) is a gas-phase reaction that allows converting two GHG- CO_2 and methane (CH_4)- in syngas. However, in order to attain high product yield, the process requires high temperature (>700 ℃) and is mainly affected by catalyst thermal stability and deactivation due to sintering and coke deposition because of parasitic reactions such as Boudouard reaction (reverse Eq. (3)), methane cracking reaction (Eq. (5)), at high temperature between 570-700 ℃) and carbon gasification (Eq. (6)), which degrades long-term durability and the reaction rate [10].

$$CH_4 + CO_2 \rightarrow 2\,CO\ +\ 2\,H_2,\ \ \Delta H_{298\,K} = 247.29\ \text{kJ} \cdot \text{mol}^{-1} \qquad \text{Eq. (4)}$$

$$CH_4 \rightarrow C + 2\,H_2,\ \ \ \Delta H_{298\,K} = 74.85\ \text{kJ} \cdot \text{mol}^{-1} \qquad \text{Eq. (5)}$$

$$C + H_2O \rightarrow CO\ + H_2,\ \ \ \ \Delta H_{298\,K} = 175.30\ \text{kJ} \cdot \text{mol}^{-1} \qquad \text{Eq. (6)}$$

ECR reaction happens in an electrolyzer where redox reactions occur. There are two types of electrochemical cells: galvanic/fuel/voltaic cells and electrolytic cells. The main difference is that, in the second type, the redox reactions are nonspontaneous ($\Delta G > 0$). This means that the cathode (where the reduction half-reaction happens) is the negative pole, and the anode (where the oxidation half-reaction happens) is the positive pole. Therefore, an energy source needs to be supplied to force electrons to flow from the anode to the cathode compartment. Oxidation half-reaction also generates cations that will be transferred to the cathode compartment through a separator. Table 1 summarizes several multi-electrons (from two to twelve electrons) and multi-protons transfer processes to form different products via different pathways and its thermodynamic standard potentials versus a standard hydrogen electrode (SHE) [14].

Table 1- Standard potential for ECR in aqueous media at 25 ℃ and 1 atm [14].

Reaction product	Reaction	E^0 (V vs. SHE)	
Carbon monoxide (**CO**)	$CO_2 + 2\,H^+ + 2\,e^- \leftrightarrow CO + H_2O$	-0.10	Eq. (7)
Formic acid (**HCOOH**)	$CO_2 + 2\,H^+ + 2\,e^- \leftrightarrow HCOOH$	-0.20	Eq. (8)
Oxalic acid ($\mathbf{C_2H_2O_4}$)	$2\,CO_2 + 2\,H^+ + 2\,e^- \leftrightarrow C_2H_2O_4$	-0.475	Eq. (9)
Formaldehyde ($\mathbf{CH_2O}$)	$CO_2 + 4\,H^+ + 4\,e^- \leftrightarrow CH_2O + H_2O$	-0.071	Eq. (110)
Methanol ($\mathbf{CH_3OH}$)	$CO_2 + 6\,H^+ + 6\,e^- \leftrightarrow CH_3OH + H_2O$	0.03	Eq. (11)
Methane ($\mathbf{CH_4}$)	$CO_2 + 8\,H^+ + 8\,e^- \leftrightarrow CH_4 + 2\,H_2O$	0.17	Eq. (12)
Ethylene ($\mathbf{C_2H_4}$)	$2\,CO_2 + 12\,H^+ + 12\,e^- \leftrightarrow C_2H_4 + 4\,H_2O$	0.07	Eq. (13)
Acetic acid ($\mathbf{C_2H_5OH}$)	$2\,CO_2 + 12\,H^+ + 12\,e^- \leftrightarrow C_2H_5OH + 3\,H_2O$	0.085	Eq. (14)
Propanol ($\mathbf{C_3H_7OH}$)	$3\,CO_2 + 18\,H^+ + 18\,e^- \leftrightarrow C_3H_7OH + 5\,H_2O$	0.09	Eq. (15)

2.1.2 Oxalic acid

It seems more promising to produce oxalic acid through an electrochemical pathway than CO because it allows to obtain a higher amount of carbon per amount of product, thus making it more valuable, and also because oxalic acid seems to be the simplest C_{2+} product to be synthesised, requiring the lowest energy input.

Oxalic acid is the simplest saturated dicarboxylic acid existing as white and odorless crystals in both dihydrate form ($C_2H_2O_6$, 71.42 wt% oxalic acid and 28.58 wt% water) and anhydrous form ($C_2H_2O_4$). The second being obtained from the first by a crystallization and/or drying process. Some of the main physical and chemical properties of anhydrous oxalic acid are presented in Table 2. It presents great commercial and industrial potential having several applications regarding metal treatment (~ 28 %), textile treatment (~ 25 %), in addition to being applied as a tanning and bleaching agent due to its ability to form readily soluble iron(III) salts (~ 20 %). Since it is a strong dehydrating agent, it can also be used to produce other chemical products (~ 27 %) such as glyoxylic acid, glyoxylate, glycolic acid, glycolate, glyoxal, glycolaldehyde, ethylene glycol, acetic acid, acetaldehyde, ethanol, ethane, ethylene, and certain metal oxalates through condensation, secondary alcohols esterification to esters, or Navarov cyclization [16, 17].

There are several methods to produce oxalic acid, but only a few of them are currently used at an industrial scale, namely nitric acid (HNO_3) based methods - oxidation of carbohydrates, oxidation of ethylene glycol, and oxidation of propene - and oxalic acid production from CO [17]. All these processes emit CO_2. Currently, Ube industries in Japan leads the oxalic acid market, followed by Oxaquim S.A in Spain (the largest European producer which has reported a capacity of 25,000 ton·year^{-1} by September 2018 [18]), and Indian Oxalate. As an alternative to the previous methods, Liquid Light (Avantium) in Amsterdam, developed a process in which CO_2 is firstly reduced to $HCOO^-$, that subsequently passed through a thermal reactor in the presence of a base catalyst to produce oxalate, which is converted into oxalic acid by a membrane-based electrochemical acidification process. Shell Oil Company, in turn, uses a metal hydroxide to react with CO_2 to form metal bicarbonate ($MHCO_3$) that is further reduced to $HCOO^-$ [19].

Table 2- Physical properties of anhydrous oxalic acid [18, 21].

Molecular mass/ g·mol^{-1}	**Density/ g·cm^{-3}**	**Melting point/ °C**	**Boiling point/ °C**
90.03	1.9	189.5	(sublimes)
Entropy (at 25 °C)/ J·mol^{-1}·K^{-1}	**Heat of combustion (at 25 °C)/ kJ·mol^{-1}**	**Standard free energy of formation (at 25 °C)/ kJ·mol^{-1}**	**Henrys Law Constant (at 25 °C)/ atm·m^3·mol^{-1}**
120.08	-245.61	-697.91	1.43×10^{-10}
Solubility	Very soluble in ethanol; slightly soluble in ether; insoluble in benzene, chloroform, and petroleum ether.		
Hazard Statements	Irritant, harmful if swallowed (H302), and in contact with skin (H312).		

2.2 ECR process variables

ECR process has several advantages, including the selective production of a wide range of chemicals (as previously mentioned) under ambient conditions in a single, simple, and easy to control (by adjusting the electrode potentials and the reaction temperature) on-site electrochemical step. Moreover, it is a compact system, easy to scale up, and the electricity needed to power the process can be harvested from renewable energy sources, such as wind, solar, and hydroelectric energy. Since it is of DMT interest to use an electric source of energy instead of solar energy, ECR is suggested as the best option for CO_2 reduction. Although ECR demonstrates to be a cost-competitive technology in a variety of global markets, it is still in an early stage of development, and the few existing processes require further studies and improvement [1–3]. This next section will briefly address the main variables and challenges of ECR, namely , electrolyte type, operating conditions (temperature, pressure, and pH), CO_2 feedstock, separator type, electrolyzer configuration, and electrocatalysts.

- **Electrolyte**

The electrolyte - usually consisting of an inert electrolyte or salt (supporting electrolyte), the solvent, and the electroactive species - allows ionic charge conduction between electrodes. It should have (1) high solubility for CO_2 to achieve high current densities; (2) low solubility to oxalic acid, to make downstream separation steps easier; (3) be electrochemically stable and chemically compatible with the electrode materials; (4) have low viscosity, to ensure good CO_2 mass transfer rates and, therefore, conductivity; (5) be safe; (6) easy to handle and store; (7) available; (8) have high donor number, as a measure of solvent ability to donate an electron (to increase selectivity); and (9) have high relative permittivity, i.e., electrolytes should easily dissolve and dissociate into cations and anions, which allows for high electrostatic interaction between solutes and, therefore, high ionic conductivity and ionic transfer in the cell [25, 27]. Electrolyte purity should also be considered since impurities (e.g., trace metal electrodeposited) can poison the cathode catalysts leading to selectivity losses.

Aqueous solutions are the most common electrolytes used since water fulfills the properties listed above, acting both as a proton donor and acceptor. In these conditions, H_2 evolution reaction (HER) rates (Eq. (16) and Eq. (17) - acid and neutral media, respectively) competes with the working electrode, stealing H^+ from ECR, as a parasitic reaction [26]. The problem gets worse since water abundance is higher when compared to CO_2, HER kinetics are faster, and since many ECR occur at the same potential range (-0.10 V to 0.17 V vs. SHE). Besides, CO_2 low solubility in water decreases mass transport rates [27]. This problem could be attenuated by either increasing the pressure, decreasing the temperature, using a different solvent (as discussed below), or by using 3D electrodes, such as gas diffusion electrodes (GDEs), solid polymer electrolytes, and packed-bed electrodes [29, 30].

$$2\,H^+ + 2\,e^- \leftrightarrow H_2(g) \qquad \text{Eq. (16)}$$

$$2\,H_2O + 2\,e^- \leftrightarrow H_2(g) + 2\,OH^- \qquad \text{Eq. (17)}$$

Organic solvents require lower overpotential and allow to obtain higher current density due to H^+ absence and higher CO_2 solubility. However, organic solvents are usually expensive, toxic, highly volatile, and flammable. Besides, the recycling process is usually unviable, presenting high costs and the possibility of mixing with the desired products [27].

Ionic liquids (ILs) are mostly molten salts, i.e., salts in the liquid state, usually used at relatively high temperatures, hence have the capability to flow and conduct charges at the same time [27, 31]. ILs have high CO_2 solubility and selectivity, high ionic conductivity, low vapor pressure, excellent thermal stability through a wide electrochemical potential range and, in some cases, can form a stable complex with the $CO_2^{\bullet -}$ intermediate and lower the activation energy barrier. The main disadvantage of ILs is their high viscosity, which limits CO_2 diffusion rates and decreases current density. To overcome these problems, ILs could be mix with a co-solvent [27]. Also, it has been noticed that two of the most commonly used ILs (imidazolium and pyridinium-based ILs) are not as environmentally friendly as previously thought because they tend to accumulate in the systems as a result of their relatively high solubility and stability in water and their poor biodegradability [31]. Additionally, ILs have demonstrated to be unstable, decomposing at high current densities [32].

Deep eutectic solvents (DESs) show similar physicochemical properties to ILs, but are much cheaper - can be prepared from accessible and inexpensive chemicals -, and safer - DESs are biodegradable, recyclable, and have low toxicity, especially the ones derived from ChCl and renewable chemicals. Plus, DESs are easier to prepare than ILs, which generally require large amounts of salts and solvents, by just mixing a quaternary ammonium or metal salt with a simple hydrogen bond donor such as acids, amides amines, and alcohols. When the two components are mixed, the melting point of the mixture is drastically reduced due to the charge delocalization between the halide anion and the hydrogen donor and, for this reason, DESs mostly exist as a liquid at or below 100 °C [31].

Regarding the specific production of oxalic acid, depending on whether a protic or aprotic solvent is chosen, the reaction mechanism can be affected. Protic solvents (such as H_2O or methanol) are directly involved in the reaction as a proton donor while aprotic solvents proceed through the formation of a $CO_2^{\bullet -}$ anion radical that can either react through nucleophilic addition of the $CO_2^{\bullet -}$ anion radical to CO_2, followed by a second electron transfer to the adduct to form CO and CO_3^{2-} (Eq. (18) or react with another $CO_2^{\bullet -}$ anion radical forming oxalate via C-C coupling (dimerization reaction) (Eq. (19) [16, 34].

$$CO_2^{\bullet -} + CO_2 \leftrightarrow (COO)_2^{\bullet -} \xrightarrow{+\,e^-} CO + CO_3^{2-} \qquad \text{Eq. (18)}$$

$$2\,CO_2^{\bullet -} \rightarrow (COO)_2^{2-} \qquad \text{Eq. (19)}$$

Moreover, when aprotic solvents are used, three more side reactions may occur, producing CO, CO_3^{2-}, and CO_2 (Eq. (20)), glycolate ($C_2HO_3^-$) (Eq. (21)), and glyoxylate ($C_2H_3O_3^-$) (Eq. (22)), as a result of the further reduction of oxalate and glycolate, respectively [34, 35].

$$CO_2^{\bullet -} + CO_2 \leftrightarrow (COO)_2^{\bullet -} \xrightarrow{+ CO_2^{\bullet -}} CO + CO_3^{2-} + CO_2 \quad \text{Eq. (20)}$$

$$(COO)_2^{2-} + 2\,H^+ + 2\,e^- \rightarrow C_2HO_3^- + OH^- \quad \text{Eq. (21)}$$

$$C_2HO_3^- + 2\,H^+ + 2\,e^- \rightarrow C_2H_3O_3^- \quad \text{Eq. (22)}$$

- **Pressure**

Higher CO_2 partial pressure promotes ECR selectivity to higher-order carbon products [21] and suppresses HER due to the increased surface coverage of ECR intermediates on the electrode surface. However, at a given temperature, mass transfer is directly affected by CO_2 solubility and partial pressure. In aqueous and organic solvent electrolytes, the relationship between these two properties exhibits a linear behavior, contrasting with ILs and amine solvent electrolytes with a non-linear relationship. This means that a pressure increase may not translate into an increase in solubility beyond a critical point, and neither mass transfer nor ECR rates increase. Besides, higher operational pressure increases the complexity, the construction and electrolyzer operating costs. Also, pressure balance between cathode and anode chamber prevents separator damage. If this is not possible, thicker strength fabric-reinforced membranes, or porous substrates may be used to improve the separator resistance and durability [27].

- **Temperature**

Usually, the temperature range used for ECR varies between 20-40 °C. On the one hand, a temperature increase would decrease viscosity, static laminar electrode layer, and, therefore, electrolyte and separator ohmic losses, while increasing CO_2 diffusivity, and mass transfer. However, when the temperature is too high, it negatively affects the membrane's mechanical structure. On the other hand, a temperature decrease would increase CO_2 solubility, which benefits the driving force, and increases CO_2 mass transfer [27].

- **pH**

In aqueous electrolytes, pH affects the phase stability of CO_2 according to the Pourbaix diagram (Figure 2). At lower pH (<6.5), middle pH (6.5 to 10.3), and higher pH (>10.3), the predominant carbon source is carboxylic acid (H_2CO_3), bicarbonate (HCO_3^-), and carbonates (CO_3^{2-}), respectively. Usually, the pH used in aqueous electrolytes is around 9 in an attempt to suppress HER since H^+ availability is lower.

Besides, ideally, bulk electrolyzer and cathode surface pH should differ due to the catalytic reaction (OH^- production and H^+ consumption) and diffusion limitations. Thus, enhancing the mass transport will affect the activity and selectivity of the cathodic reaction since the pH difference is smaller [27].

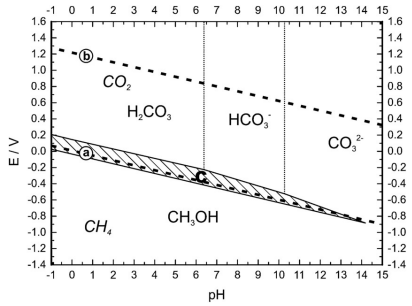


Figure 2- Pourbaix diagram for carbon at 25 °C considering predominate gaseous species (italic) and solution phase species as well as (a) lower stability window of water (HER) and (b) upper stability limit of water (O_2 evolution reaction (OER)) [35].

- **CO_2 feedstock**

The main obstacle regarding the CO_2 molecule is that it is thermodynamically very stable ($\Delta H_{298\,K}$= - 393.50 kJ·mol^{-1} [36]), which means that the energy required to break the molecule's bonds is high [37], resulting in a harder conversion, overpotential increase, and decrease of process energy-efficiency [15]. This is felt specifically for the first elementary step in the reduction (chemical adsorption of CO_2 molecules on the cathode surface and formation of the CO_2 anion radical) which is considered the rate-limiting step (Eq. (23)) [28]. Additionally, the molecule has a linear and symmetrical structure (non-polar molecule) which disfavors its adsorption, it is considered a large molecule, and has low solubility in water (30 mM at ambient temperature and 1 atm [28]) which limits CO_2 mass transfer from the gas phase to the bulk electrolyte, to the cathode/electrolyte interface, followed by its adsorption at the cathode surface active sites [37].

	E^0 (V vs. SHE)	
$\mathbf{CO_2(g) \rightarrow CO_2(ads) + e^- \rightarrow CO_2^{\bullet -}(ads)}$	-1.90 (water) or -1.97 (organic solvents)	Eq. (23)

- **Separator**

Despite increasing cell cost, complexity, and the required cell potential for a given current density due to the cell resistance increment, the separator fulfills several purposes, namely (1) prevents oxidation and reduction products crossover, which may form unsafe/unstable mixtures and make downstream steps more difficult, (2) maintains desired local conditions in the anode and cathode reactions, (3) provides mechanical support to withstand any pressure differences between chambers, (4) mediates selective ion transport from one half-reaction to another, (5) prevention of parasitic redox shuttle (i.e., reactions involving reduction of a species at the cathode followed by its reoxidation at the anode), and (6) prevents electrodes contact, hence short circuit [37].

Two main separator types can be distinguished: porous separators- including plastic mesh and microporous separators or diaphragms- and ion exchange membranes (IEM)- including monopolar separators, i.e., cation exchange membranes (CEM) and anion exchange membranes (AEM), and bipolar membranes (BPM) (Figure 3) [37].

Porous separators are open structures. Plastic meshes (e.g., polyolefin or Netlon) have large pores between 0.5-12 mm and are used as support for fragile electrodes, membranes, and/or microporous separators, to promote turbulence and thus, enhancing mass transfer near the electrodes. Besides, they offer little or inexistent resistance to anolyte and catholyte mixing. Microporous separators (e.g., glass fibres, porous polyvinyl chloride, and polytetrafluoroethylene) have pore sizes between 0.1–50 µm and acts both as convection and diffusion barriers being permeable to solvent, solute, and ions [25, 38].

IEM are typically a thin sheet of polymer with ion-exchange groups (anions in the case of CEM and cations in the case of AEM) distributed throughout their structure and with pore sizes in the range of 10^{-9} to 10^{-8} m which divides the cell into two hydraulically separated compartments [24]. CEM (e.g., Nafion®), also referred to as proton exchange membranes, allow cations (H^+) transport from anolyte to the catholyte while AEM (e.g., Fumasep®) allow anions transport in the opposite direction. BPM facilitates water dissociation into OH^- and H^+ under reverse bias, driving them to the anode and cathode, respectively. This allows to achieve more stable pH levels between the two electrodes, besides enabling the use of more economically viable electrocatalysts [25, 38].

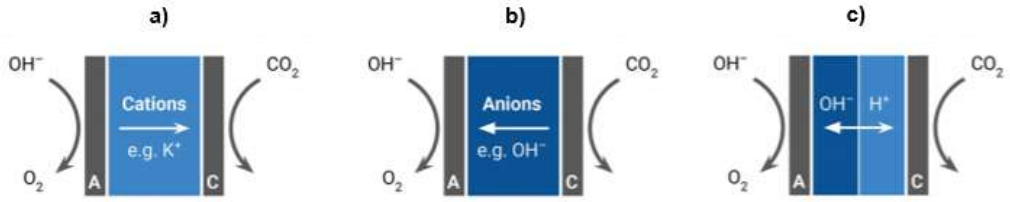


Figure 3- Different types of ion exchange membranes (IEM): a) CEM, b) AEM, and c) BPM. The letters A and C stand for anode and cathode, respectively. Adapted from [38].

- **Electrolyzer configuration**

Different types of electrolyzers can be distinguish depending on the number of compartments considered (one, two, three-compartments cell), how CO_2 is feed to the cell, as well as electrolyte phase. CO_2 can be fed either as a liquid, i.e., dissolved in the catholyte solution, or added in its ionic form (which happens outside the electrolyzer thus, requires an extra step for CO_2 capture), or it can be fed directly as a gas by using a GDE which allow to overcome/alleviate CO_2 mass transfer limitations from the gas phase to the cathode-catholyte interface. In this situation (vapor-fed electrolyzer, (Figure 4-c) a membrane electrode assembly (MEA), which consists on placing of position the PEM between a cathode GDE and an anode GDE, which is usually prepared through a hot press process. Hence, the MEA is assembled in between the anode and cathode current collectors and flow field plates [35]. To obtain the cathode and anode GDEs, a gas diffusion layer must be integrated with the catalytic layer [37]. Solid phase electrolyte (characteristic of SOEC reactors) can also be used, as explained below.

The three common reactor configurations are batch (or semi-batch) cell (H-cell), continuous flow-cell, and differential electrochemistry mass spectrometry (DEMS) cell [39]. The main characteristics of each reactor are briefly presented below. A detailed description of the main pros and cons is presented in Table A 1.

1. H-cells (Figure 4-a) are the most common configurations and include both conventional and sandwich cells. In conventional H-cells cathode and the reference electrodes (used for potential measurement) are parallelly placed in a cathodic chamber, while the anode is set in an anodic chamber but closed to the cathode. The chambers are usually connected through a circular channel and separated by a membrane in a typical "H" form. CO_2 is continuously fed into the cathodic chamber via a glass frit, and liquid products formed are accumulated in the electrolyte while gas phase products are collected from the headspace. The main difference to the sandwich cell is that, in the latter, the cathode and anode electrodes are packed in between two plates instead of being inserted into the electrolyte [39].

2. Continuous flow-cell electrolyzers are mainly used at an industrial scale in which large volumes of CO_2 need to be treated to achieve satisfactory reaction rates and ensure process economic viability [37]. There are different possible flow-cell electrolyzers configurations such as:
   2.1. Polymer electrolyte membrane (PEM) cells which only use two electrodes (the reference electrode is not used). Thus, current is usually applied to control the reaction instead of potential [39]. Catholyte/CO_2 flow-rate are the key metric of these electrolyzers and directly affects mass transfer and reaction rates [37].
   2.2. In a microfluidic flow cell (MFC) (Figure 4-d), a gas stream of CO_2 is fed into the cathode and directly contacts with a porous gas diffusion layer, while O_2 is feed to the anode side. The cathode and anode are separated by a very thin channel (<1 mm) where the electrolyte flows. The products and excess protons formed at the cathode and anode, respectively, can be carried out of the reactor with the electrolyte stream [39].
   2.3. Solid-oxide electrolysis cell (SOEC) reactors use gaseous inputs, which are feed through porous and diffusive ceramic materials (solid cathode and anode), with a solid electrolyte (usually a layer of solid oxide) for ion conduction at temperatures between 300 ℃ and 1,500 ℃ [21]. SOEC can usually be divided into oxygen ionic conductors- where CO_2 and H_2O are fed to the cathode and reduced to the desired product and oxygen ions, respectively; then, oxygen ions pass through the membrane to the anode and are oxidized to O_2-or protonic conductors- where CO_2 and H_2O are fed to cathode and anode, respectively; H_2O is oxidized to O_2 and the resulting protons pass through the membrane to the cathode to allow ECR [39].

3. In a DEMS cell, the cathode and anode are set parallel and separated by a pervaporation membrane. This way, it is possible to guarantee uniform potential distribution on the electrodes' surface while reaction products are collected in real-time and in a continuously and efficient way [39].

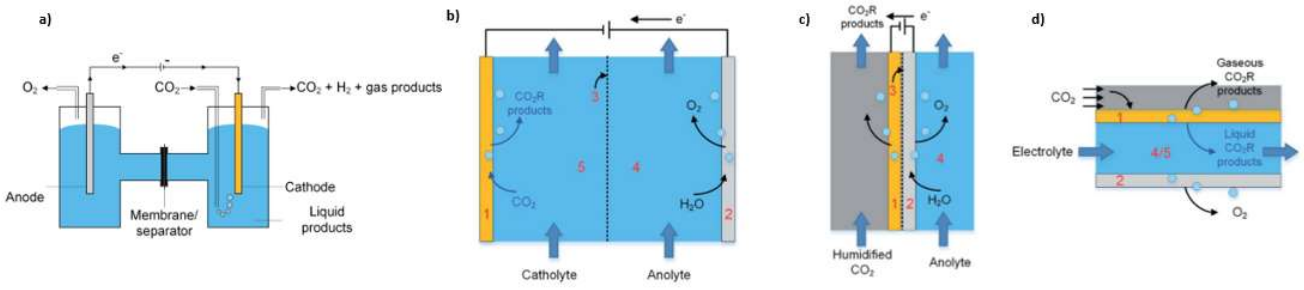


Figure 4- Schematic representation of a) conventional H-cell reactor; b) two chambers liquid-fed electrolyzer; c)- vapor-fed electrolyzer; and d) microfluidic reactor. The numbers stand for: (1) cathode, (2) anode, (3) separator, (4) anolyte, and (5) catholyte. Adapted from [10, 38]

- **Electrocatalysts:**

ECR to form C_{2+} products (such as oxalic acid) need to be well controlled because of the multi proton/electron transfer steps. Therefore, many electrocatalysts have been studied and reported [40]. Metal electrocatalysts are the most studied type of electrocatalyst because they are structurally simple, easy to handle, and robust. The catalysts can be divided into groups considering the target product desired and the type of electrolyte solution used, as summarized in Table 3.

Table 3- Main products obtained with different metal electrocatalysts in both aqueous and non-aqueous electrolyte solutions [9, 15].

Electrolyte	Electrocatalyst	Product
Aqueous	Group I (e.g., Sn, Pb, In, Hg, Cd, and Bi)	not able to adsorb $CO_2^{\bullet-}$ intermediate, thus tend to be protonated at the carbon atom allowing to produce $HCOO^-$
	Group II (e.g., Ag, Au, Pd, Gd and Zn)	capable of bonding with $CO_2^{\bullet-}$ and, thus tend to be protonated at the oxygen atom, releasing CO
	Group III (e.g., Ni, Ti, Fe and Pt)	have low HER overpotentials and strong CO adsorption properties, leading to H_2 as the main product
	Al, Ga, and Group VIII (except Pd)	(weak performance)
Non-aqueous	Pb, Tl, and Hg	$(COO)_2^{2-}$
	Cu, Ag, Au, In, Zn, and Sn	CO and carbonate ions
	Ni, Pd, and Pt	CO
	Al, Ga, Group VIII (except Ni, Pd, and Pt)	CO and $C_2H_2O_4$

2.3 House of quality

To compare and position the different functional requirements regarding electrolyte, cathode, and anode for ECR to $C_2H_2O_4$, a "House-of-Quality" benchmark study (Appendix B -) was carried out. Each functional requirement was scored from 1 (lowest) to 5 (highest) according to the improvement direction of each customer requirement.

- **Cathode:**

Ikeda and co-workers [34] studied the selective production of $C_2H_2O_4$ in nonaqueous solution with various electrodes (-2.8 V vs. Ag/AgCl (0.01 M LiCl + 0.1 M TEAP)/PC in 0.1 M TEAP/PC at 100 C). The authors concluded that Lead (Pb), Thallium (Tl), and Mercury (Hg) were suitable electrocatalysts (as previously mentioned) and noticed that, in these conditions, trace amounts of CO, glyoxalic acid, and HCOOH were also formed, as shown in Table 4. Besides being the most studied electrode, Pb enables both high Faraday efficiencies (η_{FE}) and current densities (i) (max 96.8 % [41] and 800 $A \cdot m^{-2}$, when using GDE [15], respectively), and has high H_2 evolution overpotential (as desired for cathode materials) [41]. Therefore, Pb was scored with a 5, while the other cathodes were scored in decreasing order.

Table 4- η_{FE} and products obtain using selective electrocatalysts to oxalic acid production at 2.8 V vs. Ag/AgCl/(0.01 M LiCl + 0.1 M TEAP)/PC in 0.1 M TEAP/PC, and at 100 C [34].

Electrodes	Products obtained/ µmol			
	$C_2H_2O_4$	Glyoxalic acid	HCOOH	CO
Pb	397 (η_{FE}≈ 80 %)	15	13	53
Tl	365 (η_{FE}≈ 70 %)	5	11	16
Hg	312 (η_{FE}≈ 60 %)	5	6	92

None of the materials needed special storage conditions and can be stored at ambient conditions. However, special attention should be given to hazard statements. The three materials are identified as serious health hazard chemicals, Tl and Hg are also identified as toxic chemicals, and Hg is additionally classified as dangerous to the aquatic environment.

Regarding the cost, a comparison has shown that Hg is the cheapest material (Hg 99.9998 % (454 g) from Alfa Aesar by Thermo Fisher Scientific has a cost of 128.0 € [42]), followed by Pb (Pb-Lead Plate 99.998 %, 50 cm x 50 cm (≈7.1 g), 0.25 mm thick from Alfa Aesar by Thermo Fisher Scientific has a cost of 336.0 € [43]) and Tl (Tl rod, 99.999 %, 150 mm (≈225 g), 12.7 mm diameter from Alfa Aesar by Thermo Fisher Scientific has a cost of 1,952 € [44]).

- **Anode:**

Two metals were considered suitable to be used as anode: platinum (Pt) and zinc (Zn), as a sacrificial anode. Pt is the most common anode material because it is highly durable under oxidative conditions and can achieve a wide potential range due to the large O_2 overpotential (as desired for anode materials). Pt with a

0.5 M H_2SO_4 anolyte acts as an electron donor allowing OER to happen. In this situation, the residence time must be controlled so that the oxalate can be extracted from the electrolyzer as soon as produced to prevent further reduction to glycolate and glyoxylate. On the other hand, when a Zn anode is used it generates both electrons and Zn^{2+} allowing the formation of an insoluble zinc oxalate (ZnC_2O_4) and thus, prevents the further reduction of oxalate to glycolate and glyoxylate [45]. Additionally, Zn anode does not require an aqueous solution which, as previously mentioned, decreases oxalic acid yield by promoting HER, thus no membrane is needed to separate anolyte and catholyte (lower costs). Considering Frijns, J. research [46], Zn anode turns up to be more selective and it allows to achieve higher current density (max η_{FE} of 96.8 % at 36 mA·cm^{-2} [41] or max 800 A·m^{-2} for a η_{FE} of 55 % [15]) when compared with Pt anode (max η_{FE} of 85.1 % at 20 A·m^{-2} [47] or max 150 A·m^{-2} for a η_{FE} of 64 % [45]).

Once again, both materials can be stored at ambient conditions. However, special attention should be given to hazard statements since both are classified as health hazard chemicals and Zn is also a flammable material.

Regarding the cost, Zn is cheaper than Pt (Zn foil, 99 %, 15 cm x 15 cm (≈255 g), 1.6 mm thick from Alfa Aesar by Thermo Fisher Scientific has a cost of 34.50 € [48] while Pt foil, 99.997 %, 25 cm x 25 cm (≈13.4 g), 1 mm thick from Alfa Aesar by Thermo Fisher Scientific has a cost of 1,735 € [49]). However, as a sacrificial anode, Zn must be replaced at a more frequent rate than Pt.

- **Electrolyte:**

Three different solvents were considered suitable to be used as electrolyte solutions: acetonitrile (AcN), propylene carbonate (PC), and 1-Ethyl-3-methylimidazolium tetrafluoroborate ([EMIM][BF4]). Thus, they were ranked taking into consideration the properties displayed in Table 5. Each property was scored considering the improvement direction of each customer's requirements, as explained before. Regarding the safety and ease of disposal of the three solvents, all three are classified as an irritant; AcN is also classified as flammable, and [EMIM][BF4] is considered hazardous to the aquatic environment.

Table 5- Electrolytes parameters.

	AcN [50]	PC [50]	[EMIM][BF4]
Relative permittivity	35.9	66.1	13.9 ± 0.4 [51]
CO_2 solubility (at 25 ºC)/ mol$_{CO2}$·L^{-1}	0.314 ± 0.006	0.134 ± 0.009	0.650 (10 atm)
Ionic conductivity/ S·m^{-1}	0.278 (30 ºC) [52]	0.521 (30 ºC) [53]	1.100 (25 ºC) [54]
Donor number (at 25 ºC)/ kJ·mol^{-1}	59.0	63.2	30.5 [55]
Viscosity/ Pa·s	3.69×10^{-4} (25 ºC) [56]	2.53×10^{-3} (20 ºC)	27.083×10^{-3} (30 ºC) [57]
Potential range/ V vs. SHE	-2.041 to 2.559 [58]	(not found)	-2.224 to 1.853 [59]

3 Materials and Methods

The methodology and tools used were based on the main questions to be answered within the scope of this project, namely:

What is the most promising way to directly convert a 250 $Nm^3 \cdot h^{-1}$ CO_2-rich feed stream of DMT's Carborex®MS into oxalic acid by an electrochemical process, considering all system variables (such as electrolytes, electrodes, voltage, cell configuration, separators, CO_2 supply, etc.)? How these variables affect the overall performance of the cell? How choosing a different electrochemical system can affect the economic viability of the process?

3.1 ECR systems considered

With these goals in mind and based on the decisions presented in the previous section, a literature review was carried out to find the process with the most potential. The two systems considered henceforward are:

1. The first approach (based on [41]) uses a Zn sacrificial anode and a Pb cathode (-2.6 V vs Ag rod electrode) in a one-cell electrolyzer with 0.1 M tetrabutylammonium perchlorate (TBAP) in AcN. It is assumed that Zn will be oxidized, react with oxalate and thus, produce zinc oxalate (ZnC_2O_4) which will be further purified to oxalic acid. The high FE achieved (96.8 % at 360 $A \cdot m^{-2}$), the lack of membrane (which decreases cell voltage since there is no ohmic resistance associated), and using an one-compartment cell are the main strengths of this approach. Besides, only zinc carbonate ($ZnCO_3$) formation is considered as a side reaction which does not represent a problem in the oxalic acid extraction process as it can be removed as the salt of concentrated acid [29]. The reactions happening in the cell are:

Approach 1		
Anode oxidation reaction	$Zn \rightarrow Zn^{2+} + 2\,e^-$	Eq. (24)
Cathode reduction reactions	$2\,Pb + 2\,CO_2 + 2\,e^- \rightarrow 2\,PbCO_2^-$	Eq. (25)
	$2\,PbCO_2^- \rightarrow (PbCO_2)_2^{2-}$	Eq. (26)
	$(PbCO_2)_2^{2-} \rightarrow 2\,Pb + (COO)_2^{2-}$	Eq. (27)
Reactions occurring in the electrolyte	$Zn^{2+} + (COO)_2^{2-} \rightarrow ZnC_2O_4\,(s)$	Eq. (28)
Side reaction	$2\,CO_2 + 2\,e^- \rightarrow CO + CO_3^{2-}$	Eq. (29)
	$Zn^{2+} + CO_3^{2-} \rightarrow ZnCO_3\,(s)$	Eq. (30)

2. The second approach (based on [45] and [46]) uses a Pt anode in 0.5 M H_2SO_4 (anolyte) and a Pb cathode (-2.7 V vs. Ag/AgCl) in contact with 0.7 M Tetraethylammonium Chloride (TEACl) in PC (catholyte). A two-chamber electrolyzer allows the reduction of CO_2 to oxalate in the cathode chamber,

which would require an additional acid-base reduction step outside the cell to produce oxalic acid. A three-chamber electrolyzer is a cheaper alternative to directly produce oxalic acid with both high η_{FE} and i (80 % and 1,200 A·m^{-2}, respectively) in the middle-compartment chamber by using the same anolyte solution, a CEM (Nafion)- to separate cathode and middle-compartment chamber,- and an AEM (Fumasep)- to separate anode and middle-compartment chamber [46]. Therefore, this will be the configuration considered. As a consequence of using an aqueous solution as anolyte, $C_2HO_3^-$, $C_2H_3O_3^-$ H_2, HCO_3^-, and $HCOOH/HCOO^-$ can also be formed [35, 61]. Since the presence of water has a negative influence on the oxalate production, for the commercial application of this process, the catholyte must be pre-treated to remove traces of water. It was assumed that the membranes can efficiently prevent water crossing. Thus, no side-reaction due to the presence of water will happen. Moreover, for the aim of this project, $(COO)_2^{2-}$ reduction to $C_2HO_3^-$ and futher reduction to $C_2H_3O_3^-$ were the only side reactions accounted. The reactions happening in the cell are:

Approach 2		
Anode/anolyte oxidation reaction	$H_2O \leftrightarrow 1/2\ O_2 + 2\ H^+ + 2\ e^-$	Eq. (31)
Cathode reduction reactions	$2\ Pb + 2\ CO_2 + 2\ e^- \rightarrow 2\ PbCO_2^-$	Eq. (32)
	$2\ PbCO_2^- \rightarrow (PbCO_2)\ _2^{2-}$	Eq. (33)
	$(PbCO_2)\ _2^{2-} \rightarrow 2\ Pb + (COO)_2^{2-}$	Eq. (34)
Reaction occuring in the middle-compartment	$(COO)_2^{2-} + 2\ H^+ \rightarrow C_2H_2O_4$	Eq. (35)
Side reactions	$(COO)_2^{2-} + 2\ H^+ + 2\ e^- \leftrightarrow C_2HO_3^- + OH^-$	Eq. (36)
	$C_2HO_3^- + 2\ H^+ + 2\ e^- \rightarrow C_2H_3O_3^-$	Eq. (37)

It should be noted that in both approaches, a supporting electrolyte was added to improve the electrolyte conductivity. In Approach 1, the conductivity of 0.1 M TBAP in AcN is 0.95 S·m^{-1} [61] (instead of just 0.25 S·m^{-1} for AcN [52]) while in Approach 2, the conductivity of 0.7 M TEACl in PC is 0.88 S·m^{-1} [45] (instead of just 0.52 S·m^{-1} for PC[53]). Additionally, the conductivity of the anolyte, the CEM, and the AEM is equal to 34 S·m^{-1}, 10 S·m^{-1}, and 5 S·m^{-1}, respectively.

Additionally, two different scenarios for each approach were considered:

a) The 250 Nm^3·h^{-1} CO_2-Carborex®MS stream will be first fed to an absorber column with the electrolyte solution and that 80 % of the fed CO_2 will be absorbed. Then, the resulting stream will be fed to the cell and, again, it will be assumed that 80 % of the CO_2 will react.
b) The 250 Nm^3·h^{-1} CO_2-Carborex®MS stream will be directly fed to the cell (through a GDE) and assuming that 80 % of the fed CO_2 will react;

It should be noted that the 80 % were assumed as being a suitable value to be considered.

3.2 Mass and energy balances

The mass flow and composition of each stream, as well as of each component inside the cell was determined according to reaction stoichiometry, selectivity, current density, and considering the CO_2 solubility in the electrolyte(s) used in each approach (0.014 $k_{CO2} \cdot L_{AcN}^{-1}$ and 5.710 $kg_{CO2} \cdot L_{PC}^{-1}$). It was assumed that the 250 $Nm^3 \cdot h^{-1}$ CO_2-rich feed stream of DMT's Carborex®MS has the composition shown in Table 6.

Table 6- Composition of the CO_2-rich feed stream of DMT's Carborex®MS.

Composition	CO_2	H_2O	CH_4	N_2	O_2	H_2S	siloxanes
Concentration	> 98.0 vol%	< 1.0 vol%	0.5-0.8 vol%	< 0.2 vol%	0.1-0.2 vol%	< 10 ppmv%	< 0.1 ppmv%

For Approach 1, the products formed in the cell (ZnC_2O_4 and $ZnCO_3$, both solid) are removed together with the electrolyte. This stream will be then purified, and ideally, all the ZnC_2O_4 will be converted to $C_2H_2O_4$ (with high recovery and purity) and the electrolyte will be recovered and recirculated to the cell again. However, since any downstream process is beyond the scope of this thesis, the reuse of the electrolyte was not accounted for in the mass balances.

For Approach 2, the products formed in the cell (O_2, $C_2H_2O_4$, OH^-, and $C_2H_3O_3^-$) are removed together from the middle compartment with the anolyte. Once again, any downstream process is beyond the scope of this thesis and thus, the anolyte recirculation was not accounted for the mass balance. Moreover, since the middle-compartment electrolyte and the anolyte are the same solution (0.5 M H_2SO_4), the amount of anolyte determined stoichiometrically was equally distributed over the two compartments and it was assumed that all the water feed will be able to flow through the CEM to the anode and react. The O_2 formed will also be able to flow to the CEM (although in the opposite direction) and will be removed along with the products and the anolyte in the middle compartment. Regarding the AEM, it was considered that $(COO)_2^{2-}$ is the only compound able to flow through the membrane. Otherwise, the electrons that reach the cathode react with H^+ promoting HER instead of the formation of $(COO)_2^{2-}$. Also, it is helpful to consider that there is no loss of catholyte through the membrane to the middle-compartment. Based on this assumption, the catholyte is recirculated to the absorber or directly to the cell (Approach 2-a) and b), respectively). However, in the former, a 10 % purge (or a 10 % regeneration stream of catholyte) is considered to keep catholyte concentration as requested and all the CO_2 not reacting (and inert gases- for Approach 2-b) is leaving the systems through that purge stream, which account 50 % of the stream leaving the cell.

The electric power consumption (*EPC*) of the ECR cell, i.e., the electrical energy needed per mass of desired product that is being produced, was determined by Eq. (38):

$$EPC = \frac{E \cdot i \cdot A}{c} \quad \text{Eq. (38)}$$

where E is the cell potential- i.e., the minimum theoretical energy needed to initiate the ECR towards a specific compound, determined as the difference between anode and cathode potentials or according to Nernst equation (Eq. (39)) [29, 63]- i is the current density (will be explained in the next sub-section), A is the area, determined by Eq. (40, and c is the mass flow.

$$E = E_A - E_C = E^0 - \frac{R \cdot T}{n \cdot F} \cdot \ln Q_r \quad \text{Eq. (39)}$$

in Eq. (39), E^0 is the standard potential, calculated as the difference between anode and cathode standard potentials ($E_A^0 - E_C^0$) or $E^0 = \frac{-\Delta G}{n \cdot F}$, R is ideal gas constant (8.314 $J \cdot K^{-1} \cdot mol^{-1}$), T is the temperature, n is the number of moles of electrons transferred in the half-cell reaction per mole of product, F is Faraday's constant (96,485 $C \cdot mol^{-1}$), and Q_r is the reaction quotient.

$$A = \frac{c \cdot n \cdot F \cdot \eta_{MM}}{i \cdot FE} \quad \text{Eq. (40)}$$

in Eq. (40), η_{MM} is the molar mass of the final product, and η_{FE} is the Faraday efficiency (will be explained in the next sub-section).

The global cell potential needed was also determined, as the sum of the cell potential and the overpotential (will be explained in the next sub-section).

The thermal flow (Q) and the temperature increase ($T_{increase}$) in the cell was also determined according to Eq. (41) and Eq. (42), respectively.

$$Q = \eta_o \cdot i \cdot A \quad \text{Eq. (41)}$$

where η_o is the ohmic overpotential (will be explained in the next sub-section)- calculated for the electrolyte (Approach 1) or the middle-compartment electrolyte (Approach 2).

$$T_{increase} = \frac{Q}{f \cdot c_p} \quad \text{Eq. (42)}$$

where f is the total flow in or out of the electrolyzer (depending on the case) and c_p is the specific heat (equal to 2.250 $kJ \cdot kg^{-1} \cdot K^{-1}$ and 1.640 $kJ \cdot kg^{-1} \cdot K^{-1}$ for Approach 1 and 2, respectively).

3.3 Parametric analysis

Before explaining the purpose of the parametric analysis, it is first necessary to understand the meaning of the variables studied. Ideally, the ECR process has good stability, high η_{FE}, and i. On the contrary, low overpotentials are desired.

System stability regarding separator degradation, electrocatalyst deactivation, and poisoning by impurities present in the electrolytes solutions or in the CO_2 feed [37] affects the process feasibility. Electrocatalyst stability can be evaluated via voltammetry cycling, galvanostatic, or potentiation polarizations to understand possible degradation mechanisms [8]. The lifetime of most systems for ECR is in the order of hundreds of hours. However, for the commercial application of these systems, it is necessary to guarantee a lifetime higher than 10,000 h [63].

The η_{FE} is a measure of electrocatalyst selectivity and the efficiency with which the charge is transferred to a system and used for ECR. It is translated by the ratio between the amount of charge used to reduce CO_2 to the desired product (according to Faraday's Law) and the amount of charge supplied (Eq. (43)) and can be affected by several parameters such as reactor configuration, electrolyte, electrode structure, electrocatalyst, and reaction conditions (pH, temperature, and pressure) [38, 65–67]. Low η_{FE} increases both operating cost and downstream purification costs due to production and separation of the undesired products formed, respectively. High η_{FE} (>80 %) are preferred.

$$\eta_{\mathrm{FE}} = \frac{z \cdot n \cdot F}{q} \cdot 100\ \% \qquad \text{Eq. (43)}$$

in Eq. (43), z is the number of moles of product formed, and q is the amount of charge supplied to the system that can be calculated as a product between the amount of total current and the amount of time this current is applied ($q = I \cdot \Delta t$). Note that, it was considered an operationg time equal to 8,000 $h \cdot y^{-1}$.

The i describes the total rate of reaction and, therefore, is an important input to estimate the electrolyzer size and capital cost for the ECR process [67]. It can be calculated by the amount of the total current per area, according to Eq. (44). However, for this project, this value was assumed based on literature. For the commercial application of ECR process, i of 1,000-10,000 $A \cdot m^{-2}$ are preferred. However, many laboratory-scale cases are limited to i between 10-100 $A \cdot m^{-2}$ because of CO_2 low solubility in aqueous conditions [21].

$$i = \frac{I}{A} \qquad \text{Eq. (44)}$$

The kinetic equations for an electrochemical process, generally known as Butler-Volmer equation (Eq. (50)), correlates i and η. In this situation, no mass-transfer limitations are assumed. However, low overpotentials (polarization resistance) as well as the following considerations must be accounted for. Firstly, i can be expressed as a function of the anode and cathode reactions in both forward and backward directions as written in Eq. (45) to Eq. (48).

Anode: $\mathrm{Red} \underset{k_b}{\overset{k_f}{\rightleftarrows}} \mathrm{Ox} + 2\mathrm{e}^-$

$$j_f = k_f \cdot [Red] \quad \text{Eq. (45)}$$

$$j_b = k_b \cdot [Ox] \quad \text{Eq. (46)}$$

Cathode: $\mathrm{Ox} + 2\mathrm{e}^- \underset{k_b}{\overset{k_f}{\rightleftarrows}} \mathrm{Red}$

$$j_f = k_f \cdot [Ox] \quad \text{Eq. (47)}$$

$$j_b = k_b \cdot [Red] \quad \text{Eq. (48)}$$

where j_f/j_b are the surface reaction speed, k_f/k_b are the kinetic reaction constants of the forward/backward reaction, and $[Red]/[Ox]$ are the molar concentration of the reduced/oxidized species, respectively. For general redox reactions, k_f/k_b can be expressed by the Arrhenius equation (Eq. (49)):

$$k_{f/b} = k_{0,f/b} \cdot \mathrm{e}^{\left(\frac{\alpha \cdot n \cdot F \cdot E}{R \cdot T}\right)} \quad \text{Eq. (49)}$$

$$i = n \cdot F \cdot \left(j_f - j_b\right) = i_0 \left[\mathrm{e}^{\left(\frac{\alpha_A \cdot F \cdot \eta_{act}}{R \cdot T}\right)} - \mathrm{e}^{\left(\frac{-\alpha_C \cdot F \cdot \eta_{act}}{R \cdot T}\right)}\right] \quad \text{Eq. (50)}$$

where i_0, the global exchange current density, is analogous to the rate constant in chemical reactions, i.e. the current at equilibrium and net current, dependent on electrode and electrolyte used, and is a measure of electrode's readiness to proceed with the electrochemical reaction; α_A and α_C are the charge transfer coefficients for anode and cathode, respectively, η_{act} is the activation overpotential (which will be explain below). Due the lack of information regarding α_A and α_C values, it was assumed α_A =[0.021; 0.258] and α_C =[0.042; 0.509] for Approach 1, and α_A = [0.023; 0.282] and α_C = [0.021; 0.257] for Approach 2.

The difference between E and E^0 is called overpotential (η) that is the driving force of the electrode reaction (the larger the overpotential, the faster the electrode reaction rate would be). It shows how far the electrode is from its thermodynamic equilibrium value or, in other words, the amount of non-reversible energy needed to overcome the energy barriers and resistances to drive the reaction. Therefore, at least three overpotential contributions should be taken into consideration as illustrated in Figure 5 and explained below:

- the concentration overpotential (η_c): the external energy required to keep concentration gradients near the electrode for the reaction because of diffusion (e.g., gas-bulk diffusion, adsorbates surface diffusion) and mass-transport limitations (e.g., bubble formation) on the surface of electrodes at high current (Eq. (51));

$$\eta_c = \frac{R \cdot T}{n \cdot F} \cdot \left[\ln\left(1 - \frac{i}{i_{L,A}}\right) + \ln\left(1 - \frac{i}{i_{L,C}}\right)\right] = \frac{R \cdot T}{F} \cdot \ln\left(1 - \frac{i}{i_L}\right) \quad \text{Eq. (51)}$$

where i_L is the limiting current density, typically varying between 1.00×10^4 to 1.50×10^4 A·m^{-2} [68] which was considered equal for anode and cathode within the aim of this project.

- the ohmic overpotential (η_o): the external energy required because of all internal resistances in the system, namely the membrane resistance, electronic resistances (neglected due to its little impact) and ionic resistances. According to Eq. (52), this energy increment can be reduced by minimizing the electrode spacing between electrodes, by using a low-resistivity separator, and/or by increasing electrolyte conductivity;

$$\eta_o = I \cdot R_o = I \cdot \frac{l}{\kappa \cdot A_0} \quad \text{Eq. (52)}$$

in Eq. (52), R_o is the ohmic resistance, κ is the electrolyte/membrane conductivity (see 3.1), l is the conducting length (equal to 0.004 m for the electrolytes, 5.00×10^{-5} m for AEM, and 1.78×10^{-4} m for CEM), and A_0 is the cross-section area.

- the activation overpotential (η_{act}): the external energy required to overcome the activation energy for products formation on the surface of electrodes at a considerable rate (Eq. (53));

$$\eta_{act} = \eta_{act,A} - \eta_{act,C} \quad \text{Eq. (53)}$$

where $\eta_{act,A}$ and $\eta_{act,C}$ are the anode and cathode (negative) activation overpotentials, respectively.

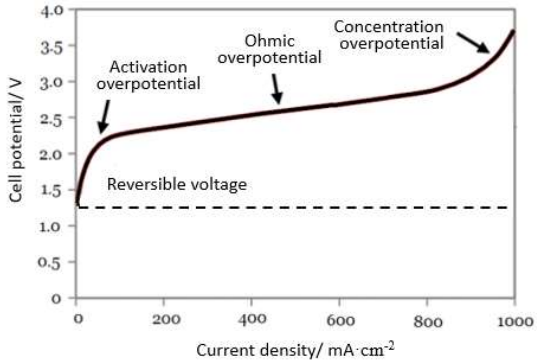


Figure 5- Typical polarization curve as a function of current density, showing the dependent regimes controlled by the activation, concentration, and ohmic overpotentials. Adapted from [69].

When $|\eta_{act}|$> 0.050 V, the Butler-Volmer equation can be simplified to Eq. (54) which only takes into account the rate of the anodic direction (first term). A smaller slope implies that the charge transfer is higher due to an increment of current density with the increasing overpotential, which translates into a more active catalyst [8].

$$i = i_0 \left[e^{\left(\frac{\alpha_A \cdot F \cdot \eta_{act}}{R \cdot T}\right)} \right] \quad \text{Eq. (54)}$$

It should be noted that cell overall overpotential can also be affected by temperature and pressure. Based on the literature, both systems operate at atmospheric pressure (1 atm) and a temperature equal to 5 °C and 25 °C, respectively for Approach 1 and 2. Thus, the effects of temperature and pressure were not considered. In addition, a good cell design and an appropriate catalyst material modification can reduce cell overall overpotential, but it cannot be completely eliminated [28].

The parametric analysis was performed using Excel Solver tool. This tool allows to find the optimal value for a variable, which is called objective function, when subjected to constraints or limits on the value of the other(s) variable(s). The goal of the parametric analysis was to minimize the square

error (objective function) of the i calculated according to Eq. (50) and the desired value (varied it between 100-5,000 $A \cdot m^{-2}$) to study the η_{act} behaviour. Due the lack of literature available, α_A and α_C were varied in the ranges assumed, and i_0 was considered equal to 1.71×10^{-4} $A \cdot m^{-2}$ for both cathode and anode (value obtain for ECR over Ag to produce CO and H_2 [70]), 1.00 $A \cdot m^{-2}$ (random value assumed for the comparison of magnitude orders), as well as $i_{0,Pt}$= 5.00 $A \cdot m^{-2}$, $i_{0,Zn}$= 3.00×10^{-7} $A \cdot m^{-2}$, and $i_{0,Pb}$= 2.50×10^{-9} $A \cdot m^{-2}$ (values obtain for H_2 evolution reaction [71]).

3.4 **Business case**

The cost analysis for the four systems accounted the annual Capital Expenditures (CAPEX)- with regard to the cost of acquiring the equipment (absorber, cell, storage tanks, and downstream units), also known as investment CAPEX, the depreciation for 15 year $\left(\text{depreciation} = \frac{\text{equipments cost}}{15}\right)$, and a 4 % interest. The annual Operational Expenses (OPEX)- which included raw materials costs and yearly electricity consumption cost as a function of energy consumption, electricity price, and the yearly production (variable production costs), plus maintenance costs (3 % total CAPEX per year), costs associated with zinc degradation (considering 3 replacements per year), and the downstream process (fixed charges)- was also accounted. Therefore, it was possible to determine each system annual Total Cost of ownership (TCO), the profit (profit = annual TOI – revenues), and return on investment (ROI) (ROI = profit – investment CAPEX).

4 Results and discussion

4.1 Mass and energy balances

The process flow diagram (PFD) for each system considered is shown in Figure 6. The mass balance for each of the systems and the $T_{increase}$ (see Eq. (42) are presented from Table 7 to Table 10.

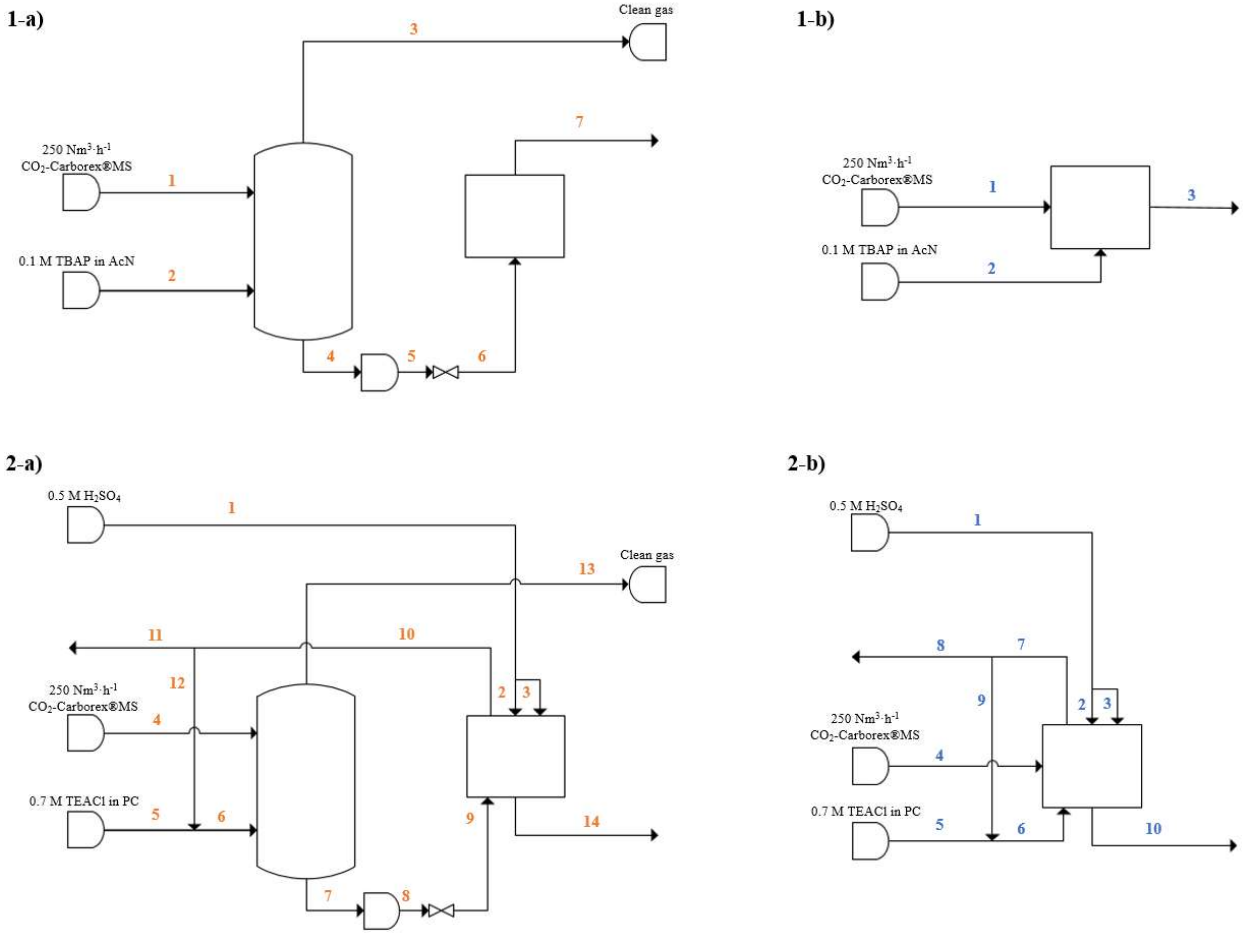


Figure 6- PFD for Approach 1-a) and b), and Approach 2-a) and b).

Table 7- Streams table for Approach 1- a).

Stream ID		Cell [a]	1	2	3	4	5	6	7
Pressure/ atm		1							
Temperature/ °C		5							25
Mass flow/ $kg \cdot h^{-1}$		225.765	478.618	22,358.457	98.805	22,738.270			22,963.901
Mass fractions/ %	CO_2	0	99.195	0	96.102	1.670			0.331
	H_2O	0	0.414	0	2.008	0			
	CH_4	0	0.184	0	0.894	0			
	N_2	0	0.129	0	0.624	0			
	O_2	0	0.074	0	0.357	0			
	H_2S	0	0.003	0	0.016	0			
	siloxanes	0	traces	0	trace	0			
	TBAP	0		3.871	0	3.806			3.769
	AcN	0		96.129	0	94.523			93.594
	ZnC_2O_4	0							2.232
	CO	0							0.013
	$ZnCO_3$	0							0.060
	Zn	1	0						

Table 8- Streams table for Approach 1- b).

Stream ID		Cell [a]	1	2	3
Pressure/ atm		1			
Temperature/ °C		5			25
Mass flow/ $kg \cdot h^{-1}$		282.206	478.618	28,085.494	28,846.150
Mass fractions/ %	CO_2	0	99.195	0	0.329
	H_2O	0	0.414	0	0.007
	CH_4	0	0.184	0	0.003
	N_2	0	0.129	0	0.002
	O_2	0	0.074	0	0.001
	H_2S	0	0.003	0	traces
	siloxanes	0	traces	0	traces
	TBAP	0		3.852	3.751
	AcN	0		96.148	93.612
	ZnC_2O_4	0			2.221
	CO	0			0.013
	$ZnCO_3$	0			0.060
	Zn	1	0		

[a] To "close" the mass balance for the global system it was necessary to account for the amount of Zn that needs to be added at each replacement.

Table 9- Streams table for Approach 2-a).

Stream ID		1	2	3	4	5	6	7	8	9	10	11 [b]	12 [c]	13	14
Pressure/ atm		1													
Temperature/ °C		25					25				179		25		27
Mass flow/ $kg \cdot h^{-1}$		78.308	39.154		478.617	5.973	135.693	439.543			211.655	81.936	129.7120	98.804	382.117
Mass fractions/ %	CO_2	0			99.195	0	55.981	86.411			71.780	92.710	58.559	96.102	0
	H_2O	95.325			0.414	0								2.008	0
	CH_4	0			0.184	0								0.894	0
	N_2	0			0.129	0								0.624	0
	O_2	0			0.074	0								0.357	17.345
	H_2S	0			0.003	0								0.016	0
	siloxanes	0			traces	0								trace	0
	TEACl	0				12.917	5.686	1.755			3.645	0.942	5.353	0	
	PC	0				87.083	38.333	11.834			24.575	6.348	36.088	0	
	H_2SO_4	4.675													0.958
	$C_2H_2O_4$	0													65.067
	$C_2H_3O_3^-$	0													13.558
	OH^-	0													3.072

Table 10- Streams table for Approach 2-b).

Stream ID		1	2	3	4	5	6	7	8	9 [c]	10
Pressure/ atm		1									
Temperature/ °C		25						218		25	31
Mass flow/ $kg \cdot h^{-1}$		81.582	40.791		478.618	7.466	173.467	272.272	94.953	166.001	477.712
Mass fractions/ %	CO_2	0			99.195	0	54.738	69.749	89.350	57.200	0
	H_2O	95.312			0.414	0	1.144	1.457	1.867	1.195	0
	CH_4	0			0.184	0	0.509	0.648	0.831	0.532	0
	N_2	0			0.129	0	0.355	0.453	0.580	0.371	0
	O_2	0			0.074	0	0.203	0.259	0.331	0.212	17.343
	H_2S	0			0.003	0	0.009	0.012	0.015	0.010	0
	siloxanes	0			traces	0	trace				0
	TEACl	0				12.917	5.560	3.542	0.908	5.229	0
	PC	0				87.083	37.482	23.880	6.118	35.251	0
	H_2SO_4	4.688									0.961
	$C_2H_2O_4$	0									65.058
	$C_2H_3O_3^-$	0									13.556
	OH^-	0									3.071

[b] A 50 % purge (stream 11 or stream 8) was considered to remove all the CO_2 that is not reacting, as well all the inert gases in Approach 2-b). Regarding the catholyte, to keep its concentration in the values needed, a regeneration stream (stream 5) accounting for 10 % of the total amount of catholyte needed is added. Therefore, 10 % of the catholyte is purged through stream 11 or stream 8.

[c] Despite the temperature increment for the catholyte, it was considered that the recirculated stream would be recirculated at ambient temperature.

Additionally, a schematic representation of the cells is shown in Figure 7. The mass balance for each component within the electrolytic cell is presented from Table 11 to Table 14.

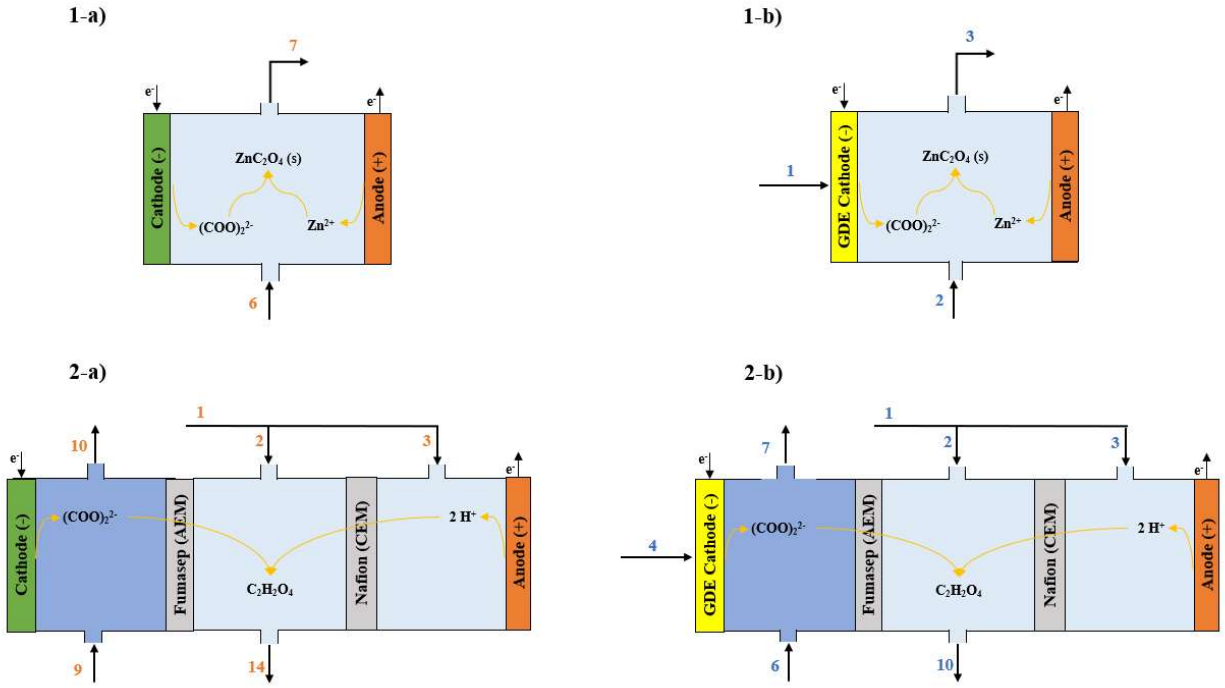


Figure 7- Schematic representation of the cells for Approach1-a) and b), and Approach 2-a) and b).

Table 11- Mass balances ($kg \cdot h^{-1}$) to components within the electrolytic cell for Approach 1- a).

Approach 1- a)

Oxidation reaction					Zn	$\rightarrow$	Zn^{2+}	+	$2\ e^-$	
					256.959		255.696			
Reduction reactions	$2\ Pb$	+	$2\ CO_2$	+	$2\ e^-$	$\rightarrow$	$2\ PbCO_2^-$			
	1,384.758		294.127				1,858.596			
					$2\ PbCO_2^-$	$\rightarrow$	$(PbCO_2)_2^{2-}$			
					1,858.596		929.298			
					$(PbCO_2)_2^{2-}$	$\rightarrow$	$2\ Pb$	+	$(COO)_2^{2-}$	
					929.298		1,384.758		294.124	
Middle-compartment			Zn^{2+}	+	$(COO)_2^{2-}$	$\rightarrow$	ZnC_2O_4			
			218.474		294.124		512.534			
Side reactions			$2\ CO_2$	+	$2\ e^-$	$\rightarrow$	CO	+	$(CO_3)^{2-}$	
			9.723				3.094		6.628	
			Zn^{2+}	+	$(CO_3)^{2-}$	$\rightarrow$	$ZnCO_3$			
			7.222		6.629		13.850			

Table 12- Mass balances ($kg \cdot h^{-1}$) to components within the electrolytic cell for Approach 1- b).

Approach 1- b)

Oxidation reaction					Zn	$\rightarrow$	Zn^{2+}	+	$2\ e^-$	
					282.120		282.120			
Reduction reactions	$2\ Pb$	+	$2\ CO_2$	+	$2\ e^-$	$\rightarrow$	$2\ PbCO_2^-$			
	1,730.947		367.659				2,323.245			
					$2\ PbCO_2^-$	$\rightarrow$	$(PbCO_2)_2^{2-}$			
					2,323.245		1,161.623			
					$(PbCO_2)_2^{2-}$	$\rightarrow$	$2\ Pb$	+	$(COO)_2^{2-}$	
					1,161.623		1,730.947		367.655	
Middle-compartment			Zn^{2+}	+	$(COO)_2^{2-}$	$\rightarrow$	ZnC_2O_4			
			273.092		367.655		640.668			
Side reactions			$2\ CO_2$	+	$2\ e^-$	$\rightarrow$	CO	+	$(CO_3)^{2-}$	
			12.154				3.868		8.286	
			Zn^{2+}	+	$(CO_3)^{2-}$	$\rightarrow$	$ZnCO_3$			
			9.028		8.286		17.316			

Table 13- Mass balances ($kg \cdot h^{-1}$) to components within the electrolytic cell for Approach 2- a).

Approach 2- a)

Oxidation reaction					H_2O	$\rightarrow$	$1/2\ O_2$	+	$2\ H^+$	+	$2\ e^-$		
					74.647		66.280		8.285				
Reduction reactions	$2\ Pb$	+	$2\ CO_2$	+	$2\ e^-$	$\rightarrow$	$2\ PbCO_2^-$						
	1,430.535		303.851				1920.037						
					$2\ PbCO_2^-$	$\rightarrow$	$(PbCO_2)_2^{2-}$						
					1920.037		960.019						
					$(PbCO_2)_2^{2-}$	$\rightarrow$	$2\ Pb$	+	$(COO)_2^{2-}$				
					960.019		1,430.535		303.847				
Middle-compartment reaction			$(COO)_2^{2-}$	+	$2\ H^+$	$\rightarrow$	$C_2H_2O_4$						
			243.078		5.523		248.631						
Side reactions	$(COO)_2^{2-}$	+	$2\ H^+$	+	$2\ e^-$	$\rightarrow$	$C_2HO_3^-$	+	OH^-				
	60.769		1.381				50.400		11.737				
	$C_2HO_3^-$	+	$2\ H^+$	+	$2\ e^-$	$\rightarrow$	$C_2H_3O_3^-$						
	50.400		1.381				51.809						

Table 14- Mass balances ($kg \cdot h^{-1}$) to components within the electrolytic cell for Approach 2- b).

Approach 2- b)

Anode oxidation reaction					H_2O	$\rightarrow$	$1/2\ O_2$	+	$2\ H^+$	+	$2\ e^-$		
					93.309		82.850		10.356				
Cathode/catholyte reduction reactions	$2\ Pb$	+	$2\ CO_2$	+	$2\ e^-$	$\rightarrow$	$2\ PbCO_2^-$						
	1,788.169		379.813				2,400.047						
					$2\ PbCO_2^-$	$\rightarrow$	$(PbCO_2)_2^{2-}$						
					2,400.047		1,200.024						
					$(PbCO_2)_2^{2-}$	$\rightarrow$	$2\ Pb$	+	$(COO)_2^{2-}$				
					1,200.024		1,788.169		379.809				
Middle-compartment reaction			$(COO)_2^{2-}$	+	$2\ H^+$	$\rightarrow$	$C_2H_2O_4$						
			303.847		6.904		310.789						
Side reactions	$(COO)_2^{2-}$	+	$2\ H^+$	+	$2\ e^-$	$\rightarrow$	$C_2HO_3^-$	+	OH^-				
	75.962		1.726				63.000		14.671				
	$C_2HO_3^-$	+	$2\ H^+$	+	$2\ e^-$	$\rightarrow$	$C_2H_3O_3^-$						
	63.000		1.726				64.761						

From the cell potential, it was possible to estimate the EPC. The Q (see Eq. (41) was calculated accounting the different contributions of ohmic overpotential. Additionally, the total cell voltage (which includes the overpotential) was determined. Table 15 summarizes the results obtained.

Table 15- Energy considerations of Approach 1 and 2.

	Approach 1	**Approach 2**
***E*/ V vs. SHE**	3.560	4.127
***EPC*/ kWh·kg^{-1}**	1.285	3.071
η_o/ V	Electrolyte: 1.516	Catholyte: 5.455 [d] CEM: 0.021 AEM: 0.012
***Q*/ kW**	Electrolyte: a) 280.482 b) 350.602	Catholyte: a) 1,010 b) 1,263 Middle-compartment: a) 29.208 b) 36.509
Total cell voltage/ V	5.076	9.756

Only from an energetic point of view, Approach 1 is better as it requires almost three times less energy which is considered an advantage since for electrochemical processes, the consumption of electricity has a large contribution to the total production cost [72]. The cell's total voltage is also almost half than that needed for the other approach.

[d] The ohmic overpotential of the catholyte in Approach 2 is clearly higher when compared with the other results obtain. This is due the conductivity considered for the catholyte (equal to 0.88 S·m^{-1} [45]) which directly affect Q and, therefore, $T_{increase}$ calculations for stream 10 and 7 of Approach 1 and 2, respectively.

4.2 Parametric analysis

Table 16 gathers all the assumptions, values collected after the literature review, as well as all the parameters' values calculated based on the explanation and methodology adopted (see 3.2).

Table 16- Parameters considered and calculated for both Approaches 1-a) and b), and Approach 2-a) and b).

		Approach 1 [41]		**Approach 2** [45]	
***FE*/ %**		96.8		80	
***i*/ A·m^{-2}**		360		1,200	
***l*/ m**	**Anolyte=Catholyte**	0.004 [73]			
	AEM (Fumasep)	-		5.00×10^{-5} [74]	
	CEM (Nafion)	-		1.78×10^{-4} [75]	
***κ*/ S·m^{-1}**	**Anolyte**	0.95 [61]		0.88 [45]	
	Catholyte			34.00 [76]	
	AEM (Fumasep)	-		5.0 [74]	
	CEM (Nafion)	-		10 [77]	
***A_0*/ m^2**		a) 514 b) 643		a) 154 b) 193	
***i_L*/ A·m^{-2}**		[1.00×10^4; 1.50×10^4] [68]			
α		α_A = [0.021; 0.258]	α_C = [0.042; 0.509]	α_A = [0.023; 0.282]	α_C = [0.021; 0.257]
***z*/ mol**		a) 3,341.597 b) 4,176.996		a) 2,761.650 b) 3,452.063	
I/ A		a) 1.850×10^5 b) 2.313×10^5			
***q*/ C**		a) 5.329×10^{12} b) 6.661×10^{12}			

Figure 8 and Figure 9 show the results obtained for both approaches when representing η_{act} as a function of i (which was varied between 100-5,000 A·m^{-2}) and considering i_0=1.71×10^{-4} A·m^{-2} and 1.00 A·m^{-2} (equal for both cathode and anode). Further information about the graphs data can be accessed in Appendix C -.

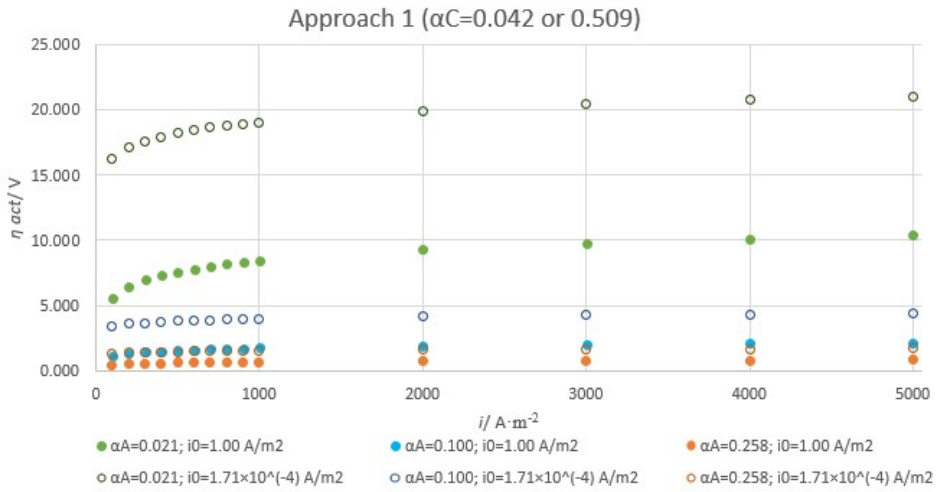


Figure 8- Parametric analysis of η_{act} as a function of i when i_0= 1.00 A·m^{-2} and 1.71 ×10^{-4} A·m^{-2} and α_A= 0.021, 0.100 and 0.258 for Approach 1.

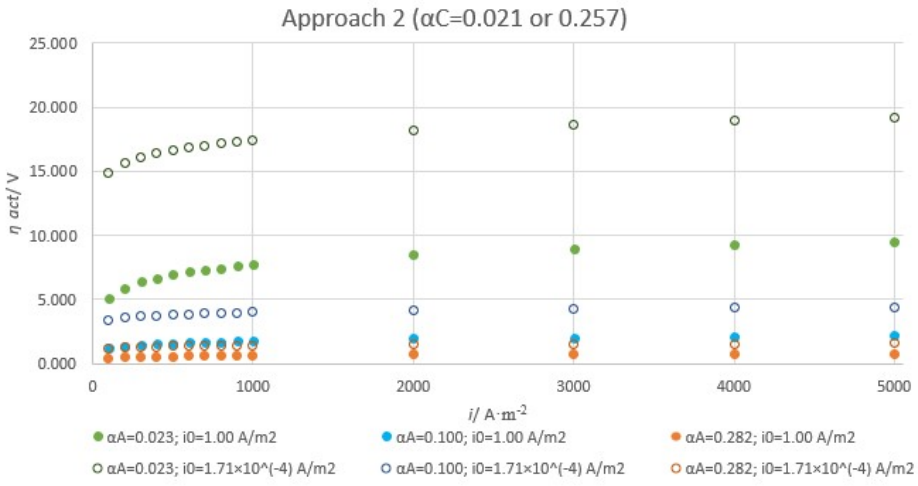


Figure 9- Parametric analysis of η_{act} as a function of i when i_0= 1.00 A·m^{-2} and 1.71 ×10^{-4} A·m^{-2} and α_A= 0.023, 0.100 and 0.282 for Approach 2.

It can be noticed that the curves obtained follow the expected profile, i.e., initially, for low i (up to 2,000 A·m^{-2}), a small increase in the voltage needed is noted but then, it reaches a plateau and remains constant.

An increase of i_0 means that the electrode is more active, thus the energy barrier the charge must overcome while moving from the electrolyte to the catalyst and vice-versa is lower, which resulted in a decrease of η_{act}. Indeed, this was the behaviour observed for both approaches. Moreover, when comparing the η_{act} voltage difference obtained for i_0=1.00 A·m^{-2} and 1.71×10^{-4} A·m^{-2} it can be notice that the lower the α_A,

the higher the η_{act} (e.g., In Approach 1, the η_{act} voltage difference is equal to 10.6 V, 2.2 V and 0.9 V for α_A equal to 0.021, 0.100 and 0.258, respectively).

Despite not being represented, i is affected only by the anodic rate direction (left part of Eq. 55), according to Butler-Volmer equation. Thus, Eq. (5 could be used as a simplification without the output being affected. Since α_C is only accounted for in the right part of Eq. 56, its contribution can be neglected, which justifies why the voltage results obtained for the minimum and maximum value of α_C are coincident.

Figure 10 and Figure 11 show the results obtained for both approaches when representing η_{act} as a function of i (varied for the same range) and considering for $i_{0,Pt}$= 5.00 A·m^{-2}, $i_{0,Zn}$= 3.00×10^{-7} A·m^{-2}, and $i_{0,Pb}$= 2.50×10^{-9} A·m^{-2}. Further information about the graphs data can be accessed in Appendix C -.

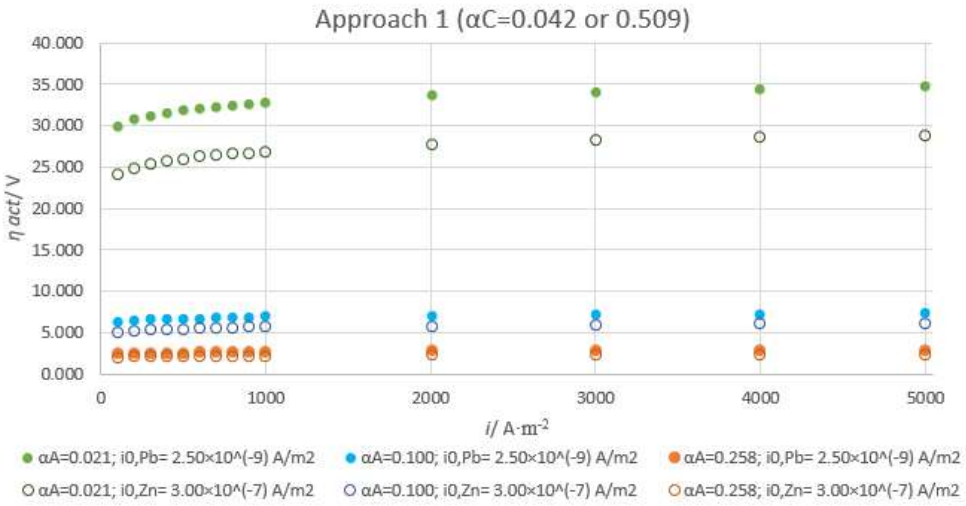


Figure 10- Parametric analysis of η_{act} as a function of i when $i_{0,Pb}$= 2.50×10^{-9} A·m^{-2} and $i_{0,Zn}$= 3.00×10^{-7} A·m^{-2} and α_A= 0.021, 0.100 and 0.258 for Approach 1.

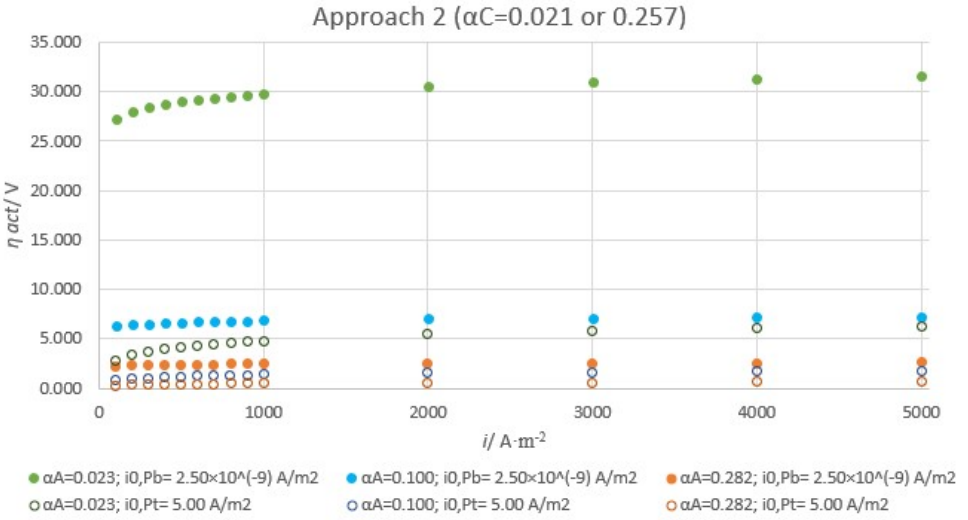


Figure 11- Parametric analysis of η_{act} as a function of i when $i_{0,Pb}$= 2.50×10^{-9} A·m^{-2} and $i_{0,Pt}$= 5.00 A·m^{-2} and α_A= 0.023, 0.100 and 0.282 for Approach 2.

Once again, the curves obtained follow the expected profile, i.e., initially, a small increase in the voltage is noted and then it seems to reach a plateau where the voltage remains constant. An increase of i_0 resulted in a decrease of η_{act}, so $\eta_{act,A}$ is always higher than $\eta_{act,C}$. Again, i calculation could also have been simplified by Eq. (5 since the curves obtained for the maximum and minimum value are coincident which means that α_C value does not affect the η_{act}. Also, when α_A decreases, the η_{act} voltage difference obtained for cathode and anode increases. This difference is mainly felt in Approach 2 (when α_A= 0.023) accounting a 25.0 V difference on average.

Since both approaches use a Pb cathode, the same analyse was carried out. The results obtained are presented in Figure 12.

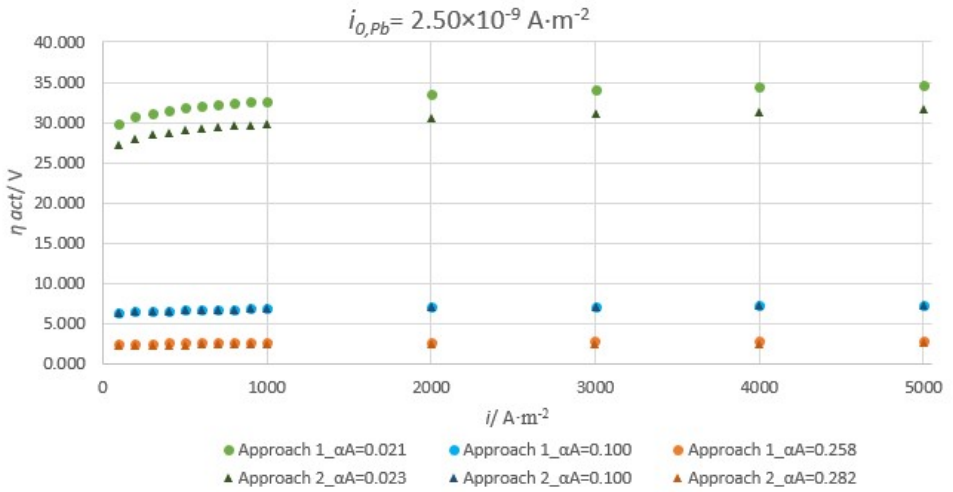


Figure 12- Comparison of the values of η_{act} for Approach 1 and 2, respectively.

As it can be observed, the difference on η_{act} values is significative only for the smallest value of α_A, accounting for 2.8 V difference on average. Also, the η_{act} is always higher for Approach 1.

4.3 Business case

With regard to investment CAPEX, electrolyzer costs present the largest weight when compared with the other equipment. Despite the significant decrease in electrolyzer costs in the last few decades, the lack of commercial-scale applications and little research and development interest concerning the reduction of its capital costs still limits the cost competitiveness of these systems. Besides, it is difficult to accurately estimate the CAPEX of the electrolytic cell as it depends on the number of configurations used, hence the number of membranes, as well as the type of electrodes incorporate. Thus, an estimated cost per area was assumed based on Ramdin and co-worker research [72] for the CAPEX cost of existing large-scale electrolyzers used for chlor-alkali and hydrogen production (assumed being similar to CAPEX cost of the CO_2 electrolyzer per unit area). For their base calculation, they have considered that a 2-compartment cell (with one membrane) that uses a GDE would cost 24,600 €·m^{-2}. All the designs considered in this thesis assume different configurations from the one previously mentioned. In this way, in line with Frijns, J. assumptions [46] and considering that adding a membrane and/or using a GDE will increase CAPEX cost, the cost considered for Approach 1-a) (1-compartment cell, no membrane, no GDE) was 16,400 €·m^{-2}, for Approach 1-b) (1-compartment cell, no membrane, GDE) was 20,500 €·m^{-2}, for Approach 2-a) (3- compartment cell, two membranes, no GDE) was 24,600 €·m^{-2}, and finally, for Approach 2-b) (3- compartment cell, two membranes, GDE) was 28,700 €·m^{-2}.

The absorber cost was determined to vary between 60,000 € to 80,000 €, as stand by Jort Langerak who, as a R&D engineer at DMT, has experience calculating columns pricing. So, an average price of 70,000 € was considered.

The choice and sizing of storage tanks took into account the standard measures available and heuristics for this type of equipment, namely a volume of liquid not more than 90 % of the total volume of the tank. In addition, at least two tanks were considered for each product, instead of only one, so that the continuity of the process would not be affected by something that happens to one of the tanks that prevent its use (for example, due to maintenance). All the tanks are at ambient pressure and temperature. The minimum volumes required and the tanks considered (in italic) are shown in Table 17. No tank was considered for the CO_2 stream as it was assumed to be directly supplied from DMT's Carborex®MS by pipeline.

Table 17- Volumes requided to be stored and corresponding tanks considered.

Volumes required/ m^3 *Tanks volumes considered/ m^3*	**Anolyte**	**Catholyte**	**Intermediate**
Approach 1-a)	32 m^3 *2×(20 m^3)*		245 m^3 *1×(161 m^3) + 1×(90 m^3)*
Approach 1-b)	40 m^3 *2×(20 m^3)*		-
Approach 2-a)	0.022 m^3 *2×(0.050 m^3)*	0.005 m^3 *2×(0.005 m^3)*	230 m^3 *1×(161 m^3) + 1×(90 m^3)*
Approach 2-b)	0.092 m^3 *2×(0.050 m^3)*	0.006 m^3 *2×(0.005 m^3)*	-

The cost of the 0.005 m^3, 0.020 m^3, and 0.050 m^3 tanks were considered to be equal to 50 €, 70 €, and 100 € [78], respectively. The costs of the 90 m^3 and 161 m^3 tanks - determined as explained in Appendix D -- were considered to be equal to 93,382 € and 119,218 €, respectively.

Downstream units also account for a large amount of the global CAPEX cost. However, any downstream process is beyond the scope of this thesis. Frijns, J. work [46] evaluated the economic feasibility of the downstream process required. Her conclusion for Approach 1 is that it will add 3,091,400 € on total CAPEX and 1,082,400 € on total OPEX per year (considering 500 $kg \cdot h^{-1}$ production of zinc oxalate production at the electrolyzer, 8000 $h \cdot y^{-1}$ operating time with a plant lifetime of 15 years). Thus, the business case directly considered these costs for Approach 1-a) and a 10 % increment for Approach 1-b) since the production is about 28 % higher than the one considered. Approach 2 counted more 1,943,400 € on total CAPEX and 787,200 € on total OPEX per year (for the same conditions). In this case, according with the production, only 50 % and 62 % of these costs were considered for Approach 2-a) and b), respectively. Although the systems considered by Frijns, J. are the same, some differences should be noted as they affect the downstream process and, therefore, limit the rigor of the estimated costs. In particular, on Approach 1 she ruled out the presence of CO, while in Approach 2 she only considered the presence of H_2O, $C_2H_2O_2$, and glycolic acid. Also, in her research, all the CO_2 fed to the cell reacts.

The high amounts of electrolyte needed, increase the costs regarding raw materials. Thus, OPEX costs are mainly dependent on that. Once again, it should be noted that as the downstream process was not the focus of this work, it was not possible to consider any recycling. In that case, the amount of solvents needed would have been lower since these, supposedly, are not consumed, only promote conductivity ionic, so could have been recycled. In addition, the price of electricity can also impact the economics of ECR depending on if a renewable or non-renewable source of energy is being used and of what kind. Renewable energy costs have continued to decrease in recent years and are increasingly more feasible when compared

with the cost of conventional fossil fuel generation. However, its intermittent behaviour, depending on capacity, region, season, market, etc., can negatively affect electricity prices and make price predictions more difficult.

As agreed in the Climate Law and the National Climate Agreement, a 49 % (95 %) reduction in greenhouse gas emissions by 2030 (by 2050) compared to 1990 levels must be achieved. To help accomplish these climate goals, the Dutch government has a 5 billion € subsidy budget available to businesses and organizations in sectors such as industry, mobility, electricity, agriculture, and the built environment. These subsidies, starting at 0.060 €·kg^{-1} (value considered) up until 300 €·t^{-1}, will be handled, as an incentive for the use of renewable energy generation techniques and other CO_2 reduction techniques [79].

Table 18 shows the prices of the raw materials, utilities, and catalyst considered for the OPEX calculation, as well as the price of the products and CO_2 incentive for the revenue's assessment of business case.

Table 18- Prices of the raw materials, utilities, catalyst, and products considered for the business case.

		Prices
Raw materials	CO_2	0.001 €·kg^{-1} [e]
	AcN	1.290 €·kg^{-1} [80]
	TBAP	2.460 €·kg^{-1} [81]
	H_2SO_4	0.050 €·kg^{-1} [82]
	H_2O	0.0002 €·kg^{-1}
	TEACL	3.280 €·kg^{-1} [83]
	PC	1.009 €·kg^{-1} [84]
Utilities	electricity	0.060 €·kWh^{-1}
Catalyst	Zn	153,33 €·m^{-2}
Product	$C_2H_2O_4$	0.705 €·kg^{-1} [f]
Incentives	CO_2	0.060 €·kg^{-1} [79]

[e] Since the CO_2 stream is being reused (before it was considered a waste stream from Carborex®MS), only a "symbolic" price was account.

[f] The price found on literature for $C_2H_2O_4$ was equal to 0.541 €·kg^{-1} [86]. However, and following Frijns, J. [46] assumptions, it is expected to be sold at a higher price since it is produced in Europe and in a sustainable way.

Table 19 shows the outcome of the cost analysis carried out for the different systems.

Table 19- Cost analysis for Approach 1-a) and b) and Approach 2-a) and b).

Cost Component	Approach 1-a)	Approach 1-b)	Approach 2-a)	Approach 2-b)
Investment CAPEX/ €				
Cell	8,429,600	13,171,271	3,793,320	5,531,925
Absorber	70,000	-	70,000	-
Storage tank	212,740	140	212,900	300
Downstream	3,091,400	3,400,540	971,700	1,204,908
	11,803,740	16,571,951	5,047,920	6,737,133
Depreciation (15 years) / €	786,916	1,104,797	336,528	449,142
Interest (4 %)/ €	274,725	385,703	117,487	156,803
Total CAPEX per year/ €	1,061,6417	1,184,921	434,867	605,918
Maintenance (3 % total CAPEX) / €	354,112	497,159	151,438	202,114
Electricity consumption per year/ €	316,131	395,164	366,503	458,128
Zn replacement per year/ €	244,260	276,000	-	-
Downstream purification/ €	1,082,400	1,190,640	393,600	488,064
Raw materials/ €				
CO_2	37,981	37,981	37,981	37,981
AcN	222,308,479	277,855,599	-	-
TBAP	17,033,375	21,291,713	-	-
H_2SO_4	-	-	1,469	1,830
H_2O	-	-	119	149
TEACl	-	-	18,232	22,766
PC	-	-	47,226	59,033
	239,379,835	299,215,294	105,023	121,760
Total OPEX per year/ €	241,376,738	301,574,256	1,010,563	1,270,066
TCO per year/ €	242,438,380	303,064,755	1,470,579	1,875,011
TCO per kg/ €	59	59	0.74	0.76
Revenues/ €				
$C_2H_2O_4$	2,890,693	3,613,366	1,402,281	1,752,851
CO_2 incentive	249,134	249,134	249,134	249,134
	3,193,827	3,862,500	1,651,415	2,001,986
Profit per year/ €	-239,298,553	-299,202,255	180,837	125,975
ROI	-0.049	-0.055	28	53

Analyzing the output of the business case, it is possible to verify that, according to the simplifications made, Approach 1 is not economically viable. Approach 2-a) allows to obtain the highest profit since it has the lowest Total CAPEX and OPEX per year (despite also having the lowest revenue). On the other hand, Approach 2-b) has a higher ROI which means that this is the most efficient investment.

5 Conclusions

The work developed in this thesis is focused on the electrochemical CO_2 reduction to produce oxalic acid. Based on a first global research on how ECR processes can be affected, two different systems for specific oxalic acid production were considered and evaluated with regard to process design (where CO_2 would be directly feed to the cell as a gas or dissolved in the electrolyte), through the realization of mass and energy balances over the global process and the electrolyzer, and determining its economic feasibility.

The first approach uses a Zn sacrificial anode and a Pb cathode (-2.6 V vs Ag rod electrode) in a one-cell electrolyzer with 0.1 M TBAP as electrolyte. It is assumed that Zn will be oxidized, react with oxalate and thus, produce solid ZnC_2O_4 which will be further purified to oxalic acid. The main advantages of this approach are the high η_{FE} achieved (96.8 % at 360 $A \cdot m^{-2}$), the lack of membrane which decreases cell voltage (only 5.076 V are needed, instead of 9.756 V for Approach 2), the use of an one-compartment cell, and producing only $ZnCO_3$ as side product, which can be easily removed. However, the low CO_2 solubility in AcN (0.014 $k_{CO2} \cdot L_{AcN}^{-1}$) significatively increased the amount of electrolyte needed when compared to the amount of catholyte needed for Approach 2 (CO_2 solubility in PC is equal to 5.710 $kg_{CO2} \cdot L_{PC}^{-1}$).

The second approach uses a Pt anode in 0.5 M H_2SO_4 (anolyte) and a Pb cathode (-2.7 V vs. Ag/AgCl) in contact with 0.7 M TEACl in PC (catholyte). A three-chamber electrolyzer was considered to directly produce oxalic acid with both high η_{FE} and i (80 % and 1200 $A \cdot m^{-2}$, respectively) in the middle-compartment chamber by incorporating a CEM and an AEM. It was assumed that $(COO)_2^{2-}$ reduction to $C_2HO_3^-$ and further reduction to $C_2H_3O_3^-$ were the only side reactions.

From the energy balances, it was also concluded that Approach 1 would be better as it requires almost three times less energy (1.285 $kWh \cdot kg^{-1}$, instead of 3.071 $kWh \cdot kg^{-1}$ needed for Approach 2).

Regarding the business case, the study of total OPEX, total CAPEX, total revenues, the profit, and the ROI of each system allowed to conclude that Approach 1 is not economically viable. Approach 2-a) achieved the highest profit (180,837 $€ \cdot year^{-1}$) while Approach 2-b) is the most efficient investment, i.e., has the highest ROI (equal to 53). Since a lot of assumptions and simplifications were made, a deeper analysis of the entire system (considering upstream processes, the reactor, and downstream processes) would be ideally recommended for a more meaningful conclusion.

Regarding the parametric analysis, it was possible to study η_{act} behaviour when the i was varied between 100-5,000 $A \cdot m^{-2}$, while varying α_A, α_C, and i_0. As expected, initially, a small increase in the voltage is noted and then it seems to reach a plateau where the voltage remains constant. Also, an increase of i_0 always resulted in a decrease of η_{act}. The value of α_C does not affect η_{act}, while a decrease in α_A value, increases η_{act}. When comparing both systems regarding the i_0 value for the cathode (since both use Pb), it was noticed that the difference on η_{act} values is significative only for the smallest value of α_A.

6 Assessment of the work done

6.1 Objectives Achieved

The scope of this work was focused on the technical assessment of an electrochemical system that can convert CO_2 into oxalic acid. The following goals were addressed and achieved during the internship:

- PFD of the process based on the research carried out;
- Mass and heat balance over the global process and the electrolyzer;
- Parametric analysis regarding the variables intrinsic to the process;
- Economic feasibility evaluation of the process;

6.2 Final Assessment

As already mentioned, the lack of research and commercial application of ECR to oxalic acid was a limiting factor for the development of the work presented. Specifically, the uncertainty regarding the mechanism and kinetics conditioned the possibility to build a mathematical model (in Aspen/ chemcad/ Matbal) that would have been used to study the system behaviour to a varying pressure, temperature, DES/IL's with CO_2 concentration, etc. So trying to find a way to overcome these obstacles was challenging. Yet, a lot of assumptions and simplifications were made. During the process, I tried to gather as much as possible the conclusions and assumptions that have been already made by other students on the same topic in order to standardize the search and make it more meaningful. I believe this was helpful not only for the purpose of my work, but also for part of the work done regarding the LCA.

Ideally, for future work, the entire system should be simulated (considering upstream processes, the reactor, and downstream processes) so that a better analysis of the feasibility and economic viability of the process can be done.

7 References

[1] "Energy consumption." https://ourworldindata.org/energy (accessed Feb., 2021).

[2] M. Steinberg, "Fossil fuel decarbonization technology for mitigating global warming," *Int. J. Hydrogen Energy*, vol. 24, no. 8, pp. 771–777, 1999, doi: 10.1016/S0360-3199(98)00128-1.

[3] "UNFCCC, eHandbook." https://unfccc.int/resource/bigpicture/ (accessed Feb., 2020).

[4] P. Mathieu, *The IPCC special report on carbon dioxide capture and storage*. 2006.

[5] and M. National Academies of Sciences, Engineering, *Gaseous Carbon Waste Streams Utilization: Status and Research Needs.* 2020.

[6] A. Chen and B. Lin, "A Simple Framework for Quantifying Electrochemical CO2 Fixation," *Joule*, vol. 2, no. 4, pp. 594–606, 2018, doi: 10.1016/j.joule.2018.02.003.

[7] C. Dioxide, "Photochemical, Electrochemical, and Photoelectrochemical Reduction of Carbon Dioxide," pp. 291–316, 2015.

[8] J. Wu, Y. Huang, W. Ye, and Y. Li, "CO2 Reduction: From the Electrochemical to Photochemical Approach," *Adv. Sci.*, vol. 4, no. 11, pp. 1–29, 2017, doi: 10.1002/advs.201700194.

[9] M. Mikkelsen, M. Jørgensen, and F. C. Krebs, "The teraton challenge. A review of fixation and transformation of carbon dioxide," *Energy Environ. Sci.*, vol. 3, no. 1, pp. 43–81, 2010, doi: 10.1039/b912904a.

[10] H. S. Whang, J. Lim, M. S. Choi, J. Lee, and H. Lee, "Heterogeneous catalysts for catalytic CO2 conversion into value-added chemicals," *BMC Chem. Eng.*, vol. 1, no. 1, pp. 1–19, 2019, doi: 10.1186/s42480-019-0007-7.

[11] "CO2 emissions." https://www.iea.org/fuels-and-technologies/hydrogen (accessed Mar., 2021).

[12] J. Y. Lee, M. Yoo, K. Cha, T. W. Lim, and T. Hur, "Life cycle cost analysis to examine the economical feasibility of hydrogen as an alternative fuel," *Int. J. Hydrogen Energy*, vol. 34, no. 10, pp. 4243–4255, 2009, doi: 10.1016/j.ijhydene.2009.03.012.

[13] S. K. Kim *et al.*, "Effect of reverse Boudouard reaction catalyst on the performance of solid oxide carbon fuel cells integrated with a dry gasifier," *Energy Convers. Manag.*, vol. 130, pp. 119–129, 2016, doi: 10.1016/j.enconman.2016.10.047.

[14] R. P. S. Chaplin and A. A. Wragg, "Effects of process conditions and electrode material on reaction pathways for carbon dioxide electroreduction with particular reference to formate formation," *J. Appl. Electrochem.*, vol. 33, no. 12, pp. 1107–1123, 2003, doi: 10.1023/B:JACH.0000004018.57792.b8.

[15] M. König, S.-H. Lin, J. Vaes, D. Pant, and E. Klemm, "Integration of the aprotic CO2 reduction to oxalate at a Pb catalyst into a GDE flow cell configuration," *Faraday Discuss.*, pp. 0–11, 2021, doi: 10.1039/d0fd00141d.

[16] E. B. Cole *et al.*, "Method and system for production of oxalic acid and oxalic acid reduction products (US9267212B2)," 2016.

[17] F. Republic and U. Industries, "Oxalic Acid," 1824, doi: 10.1002/14356007.a18.

[18] "Oxaquim S.A." https://oxaquim.com/productos-oxaquim/oxalic-acid/ (accessed Mar., 2021).

[19] M. A. Murcia Valderrama, R. J. van Putten, and G. J. M. Gruter, "The potential of oxalic – and glycolic acid based polyesters (review). Towards CO2 as a feedstock (Carbon Capture and Utilization – CCU)," *Eur. Polym. J.*, vol. 119, no. August, pp. 445–468, 2019, doi: 10.1016/j.eurpolymj.2019.07.036.

[20] "Oxalic acid- PubChem." https://pubchem.ncbi.nlm.nih.gov/compound/971#section=1H-NMR-Spectra (accessed Mar., 2021).

[21] C. Chen, J. F. Khosrowabadi Kotyk, and S. W. Sheehan, "Progress toward Commercial Application of Electrochemical Carbon Dioxide Reduction," *Chem*, vol. 4, no. 11, pp. 2571–2586, 2018, doi: 10.1016/j.chempr.2018.08.019.

[22] R. S. Costa *et al.*, "Production of oxalic acid by electrochemical reduction of CO2 using silver-carbon material from babassu coconut mesocarp," *J. Phys. Chem. Solids*, vol. 147, no. January, p. 109678, 2020, doi: 10.1016/j.jpcs.2020.109678.

[23] Y. Li and Q. Sun, "Recent Advances in Breaking Scaling Relations for Effective Electrochemical Conversion of CO2," *Adv. Energy Mater.*, vol. 6, no. 17, pp. 1–19, 2016, doi: 10.1002/aenm.201600463.

[24] J. L. Santos, D. M. F., Sequeira, C. A. C., & Figueiredo, "Hydrogen production by alkaline water electrolysis.," in *Química Nova*, vol. 36, no. 8, 2013, pp. 1176–1193.

[25] N. Solutions, E. Edition, K. I. Copyright, W. V. Gmbh, and W. Isbn, "Part One Fundamentals of Chemistry in Nonaqueous Solutions : Electrochemical Aspects," 2009.

[26] H. Ooka, M. C. Figueiredo, and M. T. M. Koper, "Competition between Hydrogen Evolution and Carbon Dioxide Reduction on Copper Electrodes in Mildly Acidic Media," *Langmuir*, vol. 33, no. 37, pp. 9307–9313, 2017, doi: 10.1021/acs.langmuir.7b00696.

[27] L. Tang, J. Liu, A. Rong, and Z. Yang, "A review of planning and scheduling systems and methods for integrated steel production," *Eur. J. Oper. Res.*, vol. 133, no. 1, pp. 1–20, 2001, doi: 10.1016/S0377-2217(00)00240-X.

[28] J. Z. Jinli Qiao, Yuyu Liu, *Electrochemical Reduction of Carbon Dioxide Fundamentals and Technologies*. .

[29] S. Subramanian, K. R. Athira, M. Anbu Kulandainathan, S. Senthil Kumar, and R. C. Barik, "New insights into the electrochemical conversion of CO2 to oxalate at stainless steel 304L cathode," *J. CO2 Util.*, vol. 36, no. August 2019, pp. 105–115, 2020, doi: 10.1016/j.jcou.2019.10.011.

[30] R. Lin, J. Guo, X. Li, P. Patel, and A. Seifitokaldani, *Electrochemical reactors for CO2 conversion*, vol. 10, no. 5. 2020.

[31] S. Khandelwal, Y. K. Tailor, and M. Kumar, "Deep eutectic solvents (DESs) as eco-friendly and sustainable solvent/catalyst systems in organic transformations," *J. Mol. Liq.*, vol. 215, pp. 345–386, 2016, doi: 10.1016/j.molliq.2015.12.015.

[32] S. S. Neubauer, B. Schmid, C. Reller, D. M. Guldi, and G. Schmid, "Alkalinity Initiated Decomposition of Mediating Imidazolium Ions in High Current Density CO2 Electrolysis," *ChemElectroChem*, vol. 4, no. 1, pp. 160–167, 2017, doi: 10.1002/celc.201600461.

[33] A. Gennaro, A. A. Isse, M. G. Severin, E. Vianello, I. Bhugun, and J. M. Savéant, "Mechanism of the electrochemical reduction of carbon dioxide at inert electrodes in media of low proton availability," *J. Chem. Soc. - Faraday Trans.*, vol. 92, no. 20, pp. 3963–3968, 1996, doi: 10.1039/FT9969203963.

[34] S. Ikeda, T. Takagi, and K. Ito, "Selective formation of formic acid, oxalic acid, and carbon monoxide by electrochemical reduction of carbon dioxide," *Bull. Chem. Soc. Jpn.*, vol. 60, no. 7, pp. 2517–2522, 1987, doi: 10.1246/bcsj.60.2517.

[35] J. R. Varcoe *et al.*, "Anion-exchange membranes in electrochemical energy systems," *Energy Environ. Sci.*, vol. 7, no. 10, pp. 3135–3191, 2014, doi: 10.1039/c4ee01303d.

[36] J. Fischer, T. Lehmann, and E. Heitz, "The production of oxalic acid from CO2 and H2O," *J. Appl. Electrochem.*, vol. 11, no. 6, pp. 743–750, 1981, doi: 10.1007/BF00615179.

[37] S. Garg *et al.*, "Advances and challenges in electrochemical CO2 reduction processes: An engineering and design perspective looking beyond new catalyst materials," *J. Mater. Chem. A*, vol. 8, no. 4, pp. 1511–1544, 2020, doi: 10.1039/c9ta13298h.

[38] D. M. Weekes, D. A. Salvatore, A. Reyes, A. Huang, and C. P. Berlinguette, "Electrolytic CO2 Reduction in a Flow Cell," *Acc. Chem. Res.*, vol. 51, no. 4, pp. 910–918, 2018, doi: 10.1021/acs.accounts.8b00010.

[39] S. Liang, N. Altaf, L. Huang, Y. Gao, and Q. Wang, "Electrolytic cell design for electrochemical CO2 reduction," *J. CO2 Util.*, vol. 35, no. September 2019, pp. 90–105, 2020, doi: 10.1016/j.jcou.2019.09.007.

[40] L. Fan, C. Xia, F. Yang, J. Wang, H. Wang, and Y. Lu, "Strategies in catalysts and electrolyzer design for electrochemical CO2 reduction toward C2+ products," *Sci. Adv.*, vol. 6, no. 8, pp. 1–18, 2020, doi: 10.1126/sciadv.aay3111.

[41] W. Lv, R. Zhang, P. Gao, C. Gong, and L. Lei, "Electrochemical reduction of carbon dioxide with lead cathode and zinc anode in dry acetonitrile solution," *J. Solid State Electrochem.*, vol. 17, no. 11, pp. 2789–2794, 2013, doi: 10.1007/s10008-013-2186-0.

[42] "10242 Mercury, Electronic Grade, 99.9998% (metals basis)." https://www.alfa.com/pt/catalog/010242/ (accessed April, 2021).

[43] "12603 Lead plate, 6.35mm (0.25in) thick, 99.9% (metals basis)." https://www.alfa.com/pt/catalog/012603/ (accessed April, 2021).

[44] "12714 Thallium rod, 12.7mm (0.5in) dia, 99.999% (metals basis)." https://www.alfa.com/pt/catalog/012714/ (accessed April, 2021).

[45] V.S.Boor, "Electrochemical reduction of CO2 to Oxalic Acid. Electrochemical conversion, downstream processing and technoeconomic analysis," TU Delft, 2020.

[46] J.E.B.M. Frijns, "Economically feasible process scale-up for the electrochemical conversion of CO2 to oxalic acid," TU Delft, 2021.

[47] Y. Cheng, P. Hou, H. Pan, H. Shi, and P. Kang, "Selective electrocatalytic reduction of carbon dioxide to oxalate by lead tin oxides with low overpotential," *Appl. Catal. B Environ.*, vol. 272, no. December 2019, p. 118954, 2020, doi: 10.1016/j.apcatb.2020.118954.

[48] "10438 Zinc foil, 1.6mm (0.063in) thick, 15x15cm (5.9x5.9in), 99% (metals basis)." https://www.alfa.com/en/catalog/010438/ (accessed April, 2021).

[49] "12060 Platinum foil, 1.0mm (0.04in) thick, Premion®, 99.997% (metals basis)." https://www.alfa.com/pt/catalog/012060/ (accessed April, 2021).

[50] M. König, J. Vaes, E. Klemm, and D. Pant, "Solvents and Supporting Electrolytes in the Electrocatalytic Reduction of

CO2," *iScience*, vol. 19, pp. 135–160, 2019, doi: 10.1016/j.isci.2019.07.014.

[51] M. M. Huang, Y. Jiang, P. Sasisanker, G. W. Driver, and H. Weingärtner, "Static relative dielectric permittivities of ionic liquids at 25 °c," *J. Chem. Eng. Data*, vol. 56, no. 4, pp. 1494–1499, 2011, doi: 10.1021/je101184s.

[52] "Ionic Conductivity of Acetonitrile." http://www.ddbst.com/en/EED/PCP/TCN_C3.php (accessed May, 2021).

[53] T. Vogl, S. Menne, and A. Balducci, "Mixtures of protic ionic liquids and propylene carbonate as advanced electrolytes for lithium-ion batteries," *Phys. Chem. Chem. Phys.*, vol. 16, no. 45, pp. 25014–25023, 2014, doi: 10.1039/c4cp03830d.

[54] V. V. Chaban, I. V. Voroshylova, O. N. Kalugin, and O. V. Prezhdo, "Acetonitrile boosts conductivity of imidazolium ionic liquids," *J. Phys. Chem. B*, vol. 116, no. 26, pp. 7719–7727, 2012, doi: 10.1021/jp3034825.

[55] M. Schmeisser and R. Van Eldik, "Elucidation of inorganic reaction mechanisms in ionic liquids: The important role of solvent donor and acceptor properties," *Dalt. Trans.*, vol. 43, no. 42, pp. 15675–15692, 2014, doi: 10.1039/c4dt01239a.

[56] "Acetonitrile." https://www.sigmaaldrich.com/chemistry/solvents/acetonitrile-center.html (accessed April, 2021).

[57] X. H. Fan, Y. P. Chen, and C. S. Su, "Density and Viscosity Measurements for Binary Mixtures of 1-Ethyl-3-methylimidazolium Tetrafluoroborate ([Emim][BF4]) with Dimethylacetamide, Dimethylformamide, and Dimethyl Sulfoxide," *J. Chem. Eng. Data*, vol. 61, no. 2, pp. 920–927, 2016, doi: 10.1021/acs.jced.5b00753.

[58] R. J. Forster, P. Bertoncello, and T. E. Keyes, "Electrogenerated chemiluminescence," *Annu. Rev. Anal. Chem.*, vol. 2, no. Cl, pp. 359–385, 2009, doi: 10.1146/annurev-anchem-060908-155305.

[59] T. Romann, O. Oll, P. Pikma, H. Tamme, and E. Lust, "Surface chemistry of carbon electrodes in 1-ethyl-3-methylimidazolium tetrafluoroborate ionic liquid - An in situ infrared study," *Electrochim. Acta*, vol. 125, pp. 183–190, 2014, doi: 10.1016/j.electacta.2014.01.077.

[60] B. Innocent, D. Liaigre, D. Pasquier, F. Ropital, J. M. Léger, and K. B. Kokoh, "Electro-reduction of carbon dioxide to formate on lead electrode in aqueous medium," *J. Appl. Electrochem.*, vol. 39, no. 2, pp. 227–232, 2009, doi: 10.1007/s10800-008-9658-4.

[61] D. Moia *et al.*, "The reorganization energy of intermolecular hole hopping between dyes anchored to surfaces," *Chem. Sci.*, vol. 5, no. 1, pp. 281–290, 2014, doi: 10.1039/c3sc52359d.

[62] S. Petrovic, *Basic Electrochemistry Concepts*. 2021.

[63] B. R. KOPER, Marc; CUENYA, "Electrochemical CO2 reduction. In Research needs towards sustainable production of fuels and chemicals." pp. 19–27, 2019.

[64] X. Zhang, S. Guo, K. A. Gandionco, A. M. Bond, and J. Zhang, "Electrocatalytic carbon dioxide reduction : from fundamental principles to catalyst design," *Mater. Today Adv.*, vol. 7, p. 100074, 2020, doi: 10.1016/j.mtadv.2020.100074.

[65] Y. Y. Birdja, E. Pérez-gallent, M. C. Figueiredo, A. J. Göttle, F. Calle-vallejo, and M. T. M. Koper, "Advances and challenges in understanding the electrocatalytic conversion of carbon dioxide to fuels," doi: 10.1038/s41560-019-0450-y.

[66] L. Fan, C. Xia, F. Yang, J. Wang, H. Wang, and Y. Lu, "Strategies in catalysts and electrolyzer design for electrochemical CO 2 reduction toward C 2 + products," no. February, pp. 1–18, 2020.

[67] C. Mesocrystals, "Stable and Selective Electrochemical Reduction of Carbon Dioxide to," 2014, doi: 10.1039/b000000x.

[68] H. J. Gores and H. Schweiger, *Encyclopedia of Applied Electrochemistry*. 2014.

[69] E. Amores, J. Rodríguez, J. Oviedo, and A. De Lucas-Consuegra, "Development of an operation strategy for hydrogen production using solar PV energy based on fluid dynamic aspects," *Open Eng.*, vol. 7, no. 1, pp. 141–152, 2017, doi: 10.1515/eng-2017-0020.

[70] M. R. Singh, J. D. Goodpaster, A. Z. Weber, M. Head-Gordon, and A. T. Bell, "Mechanistic insights into electrochemical reduction of CO2 over Ag using density functional theory and transport models," *Proc. Natl. Acad. Sci. U. S. A.*, vol. 114, no. 42, pp. E8812–E8821, 2017, doi: 10.1073/pnas.1713164114.

[71] S. Petrovic, *Electrochemistry Crash Course for Engineers*. 2021.

[72] M. Ramdin *et al.*, "High-Pressure Electrochemical Reduction of CO2 to Formic Acid/Formate: Effect of pH on the Downstream Separation Process and Economics," *Ind. Eng. Chem. Res.*, vol. 58, no. 51, pp. 22718–22740, 2019, doi: 10.1021/acs.iecr.9b03970.

[73] S. Timmerberg, M. Kaltschmitt, and M. Finkbeiner, "Hydrogen and hydrogen-derived fuels through methane decomposition of natural gas – GHG emissions and costs," *Energy Convers. Manag. X*, vol. 7, no. April, p. 100043, 2020, doi: 10.1016/j.ecmx.2020.100043.

[74] "Fumasep FAS-50." https://www.fuelcellstore.com/fumasep-fas-50 (accessed May, 2021).

[75] "Nafion 117." https://www.sigmaaldrich.com/PT/en/product/aldrich/274674?gclid=Cj0KCQjwnueFBhChARIsAPu3YkRTVYJvvrVggtzqdJ6Hr80TSG2jvF9-ZerGppPYd_7e3CZsVcxrw2gaAtU1EALw_wcB (accessed May, 2021).

[76] H. Golnabi, M. R. Matloob, M. Bahar, and M. Sharifian, "Investigation of electrical conductivity of different water liquids

and electrolyte solutions," *Iran. Phys. J.*, vol. 3, 2009.

[77] "Table 29.4. Examples of High-Temperature Proton Exchange Membrane Fuel Cell, PEMFC Membranes." https://app.knovel.com/hotlink/itble/rcid:kpAMTA000A/id:kt00CR7K94/advanced-membrane-technology/table-29-4-examples-high (accessed May, 2021).

[78] "Tanks cost." https://tanksdirekt.de/en/ (accessed June, 2021).

[79] "Stimulation of sustainable energy production and climate transition (SDE++)." https://english.rvo.nl/subsidies-programmes/sde (accessed June, 2021).

[80] "Acetonitrile bulk price." https://www.icis.com/explore/chemicals/channel-info-chemicals-a-z/# (accessed June, 2021).

[81] "Tetrabutylammonium perchlorate price." https://www.lookchem.com/product_Tetrabutylammonium-perchlorate/2040987.html#formsend (accessed June, 2021).

[82] "Helixer report for bulk prices." from DMT database (accessed June, 2021).

[83] "Tetraethylammonium Chloride price." https://www.alibaba.com/product-detail/Tetraethylammonium-Chloride-Tetraethylammonium-Chloride-Cas-56_1600127959617.html?spm=a2700.galleryofferlist.normal_offer.d_title.1d03328euDoCio&s=p (accessed June, 2021).

[84] "Propylene carbonate market price & insights." https://www.echemi.com/productsInformation/pid_Seven1855-propylene.html (accessed June, 2021).

[85] "Chemical Engineer Cost Index." https://www.chemengonline.com/site/plant%02cost-index/ (accessed June, 2021).

[86] "Oxalic acid market price & insights." https://www.echemi.com/productsInformation/temppid160705011349-oxalic-acid.html (accessed June, 2021).

Appendix A - Electrolyzer configurations

Table A 1- Summary of main advantages and disadvantages of the possible ECR electrolyzer configurations. Adapted from [11, 10, 14, 35, 36].

		Advantages	Disadvantages
H-cell	Conventional	• easy to operate and clean; • commercially available at low-cost; • mostly used at lab-scale for quick screening of electrocatalysts; • wide range of electrode options.	• low solubility of CO_2, mass transport limitations, low current densities (< 100 $mA \cdot cm^{-2}$) which does not meet commercially operationg conditions; • limitation regarding the detection of trace liquid products; • when operated for long periods, cation accumulation on the catholyte is likely to occur, leading to low electrode kinetics, low ECR selectivity, and increasing ohmic losses; • batch-cell limits mass transport.
	Sandwich	• allow high electrode surface area/electrolyte volume (S/V) ratio (usually >0.5); • lower solution resistance; • allow a better liquid products determination.	• limitation of electrodes form (plates); • mass transport limitation and bubbles formation (must be controlled by adding low-cost additives, such as propylene glycol).
Flow-cell	Polymer electrolyte membrane (PEM)	• more suitable for large-scale commercial application than H-cells; • lower cell resistance; • low-cost structural materials; ➢ vapor-fed electrolyzer: can overcome CO_2 low solubility, achieve high partial current density, stability, selectivity, lower ohmic losses, less material cost (due to reduced flowing electrolyte), and easier products separation from a liquid phase. ➢ liquid-fed electrolyzer: enhanced CO_2 diffusion with GDL, and it is possible to overcome mass transport limitations by continuously circulating the reactants and products to and away from the electrodes;	• strong corrosion by the high overpotentials. ➢ vapor-fed electrolyzer: need of humidifies CO_2 or gas flow close to the aqueous anolyte, unstable liquid outlet from the cathode, lack of a reference electrode that makes the potential measurement harder, and liquid crossover with MEA. ➢ liquid-fed electrolyzer: GDL subject to potential crystallization of salts, concentration polarization, higher ohmic loss, water issues, and contamination.
	Microfluidic flow cell (MFC)	• can operate both with or without a membrane (in the last situation, the separation of reduction and oxidation products rely on the diffusion of the gaseous products); • higher mass transport and lower ohmic losses; • flexibility in operating conditions; • minimize pH decrease and allow ECR using a strong alkaline electrolyte to achieve high current densities.	• MFC with membrane are sensitive to pressure differences making scale-up a challenge.
	Solid-oxide electrolysis cell (SOEC)	• efficient mass transport of CO_2, higher current density, selectivity, and performance.	• energy intensive (high temperature); • sensibility to system degradation; • limited to a narrow range of products (mainly to produce CO).
Differential electrochemistry mass spectrometry (DEMS) cell		• enables efficient products detection at the electrode-electrolyte interface in real-time as a function of applied voltage and local pH and CO_2 concentration near cathode surface determination; • used to study ECR mechanisms over catalysts.	• has electrodes selection, large-scale application, and mass transport limitations.

Appendix B - House of Quality

The “House of Quality” benchmark study for electrolyte, anode, and cathode is presented below in Table A 2.

Table A 2- "House of Quality".

Row #	Weight chart	Relative weight (%)	Importance (1-5)	Category	Functional Requirements / Customer requirements	Improvement direction	Electrolyte			Anode		Cathode		
							AcN	PC	[EMIM][BF4]	Pt	Zn	Pb	Tl	Hg
1		12	5	electrodes parameters	Faraday Efficiency/ %	↑				4	5	5	4	3
2		12	5		Current density/ $A \cdot m^{-2}$					4	5	5	nf	nf
3		7	3	electrolyte parameters	Relative permittivity	↑	4	5	3					
4		10	4		CO2 solubility/ $mol_{CO2} \cdot mol_{solvent}$		4	3	5					
5		10	4		Conductivity/ $S \cdot m^{-1}$		3	4	5					
6		7	3		Donor number/ $kJ \cdot mol^{-1}$ (at 25°C)	↓	4	3	5					
7		7	3		Viscosity/ Pa·s		5	4	3					
8		5	2		Potential range/ V vs. SHE		5	nf	3					
9		7	3	viability evaluation parameters	Cost/ €	↓	4	5	3	4	5	3	2	4
10		5	2		Safety and ease of disposal		3	4	3	4	3	5	4	3
					Target (1-5)		3.5	3.5	3.5	3.5	3.5	3.5	3.5	3.5
					Rating		3.0	2.7	2.9	4.0	4.7	4.6	3.4	3.3
					Relative weight (%)		10.4	9.5	10.3	14.0	16.5	16.1	11.9	11.5
					Weight chart									
					Position		1	3	2	2	1	1	2	3

nf- not found

Appendix C - Parametric analysis graphs' data

The data used to build the graphs represented in Figure 8 to Figure 12 are presented below:

		i/ A·m^{-2}	100	200	300	400	500	600	700	800	900	1,000	2,000	3,000	4,000	5,000
Approach 1 (α_C= 0.041 or 0.509)	i_0= 1.00 A·m^{-2}	α_A= 0.021	5.632	6.479	6.975	7.327	7.600	7.822	8.011	8.174	8.318	8.447	9.295	9.791	10.142	10.415
		α_A= 0.100	1.183	1.361	1.465	1.539	1.596	1.643	1.682	1.717	1.747	1.774	1.952	2.056	2.130	2.187
		α_A= 0.258	0.458	0.527	0.568	0.596	0.619	0.637	0.652	0.665	0.677	0.688	0.757	0.797	0.826	0.848
	i_0= 1.71×10^{-4} A·m^{-2}	α_A= 0.021	12.179	12.814	13.186	13.450	13.655	13.822	13.963	14.086	14.194	14.290	14.926	15.298	15.562	15.767
		α_A= 0.100	3.410	3.588	3.692	3.766	3.823	3.870	3.910	3.944	3.974	4.001	4.179	4.283	4.357	4.415
		α_A= 0.258	1.197	1.259	1.295	1.321	1.342	1.358	1.372	1.384	1.394	1.404	1.466	1.503	1.529	1.549
	$i_{0,Pb}$= 2.50×10^{-9} A·m^{-2}	α_A= 0.021	29.852	30.701	31.195	31.548	31.821	32.043	32.232	32.395	32.538	32.668	33.516	34.012	34.363	34.636
		α_A= 0.100	6.269	6.447	6.551	6.625	6.682	6.729	6.769	6.803	6.833	6.860	7.038	7.142	7.216	7.274
		α_A= 0.258	2.430	2.499	2.539	2.568	2.590	2.608	2.624	2.637	2.649	2.659	2.728	2.768	2.797	2.819
	$i_{0,Zn}$= 3.00×10^{-7} A·m^{-2}	α_A= 0.021	23.998	24.845	25.341	25.693	25.966	26.189	26.377	26.541	26.685	26.814	27.661	28.157	28.509	28.782
		α_A= 0.100	5.040	5.218	5.322	5.396	5.453	5.500	5.539	5.574	5.604	5.631	5.809	5.913	5.987	6.044
		α_A= 0.258	1.953	2.022	2.063	2.091	2.114	2.132	2.147	2.160	2.172	2.183	2.252	2.292	2.320	2.343
Approach 2 (α_C= 0.021 or 0.257)	i_0= 1.00 A·m^{-2}	α_A= 0.023	5.142	5.416	6.368	6.690	6.393	7.142	7.314	7.463	7.595	7.713	8.487	8.939	9.260	9.510
		α_A= 0.100	1.184	1.361	1.465	1.539	1.596	1.643	1.682	1.717	1.747	1.774	1.952	2.056	2.130	2.187
		α_A= 0.282	0.420	0.483	0.520	0.546	0.566	0.583	0.597	0.609	0.620	0.629	0.692	0.729	0.755	0.776
	i_0= 1.71×10^{-4} A·m^{-2}	α_A= 0.023	14.826	15.600	16.053	16.374	16.623	16.827	16.999	17.148	17.279	17.397	18.171	18.624	18.945	19.194
		α_A= 0.100	3.410	3.588	3.692	3.766	3.823	3.870	3.910	3.944	3.974	4.001	4.179	4.283	4.357	4.415
		α_A= 0.282	1.209	1.272	1.309	1.335	1.356	1.372	1.386	1.399	1.409	1.419	1.482	1.519	1.545	1.565
	$i_{0,Pb}$= 2.50×10^{-9} A·m^{-2}	α_A= 0.023	27.258	28.030	28.483	28.804	29.053	29.257	29.429	29.578	29.710	29.827	30.601	31.054	31.375	31.624
		α_A= 0.100	6.269	6.447	6.551	6.625	6.682	6.729	6.769	6.803	6.833	6.860	7.038	7.142	7.216	7.274
		α_A= 0.282	2.223	2.286	2.323	2.349	2.370	2.386	2.400	2.412	2.423	2.433	2.496	2.533	2.559	2.579
	$i_{0,Pt}$= 5.00 A·m^{-2}	α_A= 0.023	2.73	3.349	3.716	3.977	4.179	4.344	4.484	4.605	4.712	4.808	5.437	5.805	6.066	6.268
		α_A= 0.100	0.777	0.950	1.053	1.127	1.184	1.230	1.270	1.304	1.334	1.361	1.539	1.643	1.717	1.774
		α_A= 0.282	0.276	0.338	0.374	0.400	0.420	0.436	0.450	0.463	0.473	0.483	0.546	0.583	0.609	0.629

Appendix D - Storage tanks costs

The purchase cost of storage tanks (C_P) was determined according to Eq. (A 1) and then updated according to the Chemical Engineering Plant Cost Index through Eq. (A 2).

$$C_P = \mathrm{F_M} \cdot C_V + C_{PL} \quad \text{Eq. (A 1)}$$

$$C_{P,updated} = C_P \cdot \left(\frac{I}{I_{base}}\right) \quad \text{Eq. (A 2)}$$

where F_M is a material factor (equal to 1 for carbon-steel), C_V is the cost of purchasing the empty vessel (including nozzles, manholes, supports) (Eq. (A 3)), C_{PL} is the cost of adding platforms and ladders on vertical vessels for 0.914<D_i<3.658 m and 3.658<H<12.192 m (Eq. (A 4)), I_{base} is the base index for the year 2000 (equal to 394), and I is the December 2019 index (equal to 592.1 [85]).

$$C_V = \exp[8.717 - 0.23320 \cdot ln\, W + 0.04333 \cdot (ln\, W)^2] \quad \text{Eq. (A 3)}$$

$$C_{PL} = 285.1 \cdot (D_i)^{0.73960} \cdot (\mathrm{H})^{0.70684} \quad \text{Eq. (A 4)}$$

where W is the weight of the shell and two heads (Eq. (A 5)), D_i is the internal diameter, and H is the height.

$$W = \pi \cdot \rho \cdot [(r_i + t)^2 - r_i^2] \cdot H + 2\pi \cdot \rho \cdot [(r_i + t)^2 \cdot t] \quad \text{Eq. (A 5)}$$

where ρ is the mass density of carbon steel (ρ= 7,849 kg·m^{-3}), r_i is the internal radius, and t is the wall thickness, calculated by Eq. (A 6).

$$t = \frac{P \cdot r_i}{S \cdot \mathrm{E} - 0.6 \cdot P} + C \quad \text{Eq. (A 6)}$$

where P is the pressure, S is the allowable stress (equal to 10.3×10^7 Pa), E is the weld efficiency fraction (equal to 0,085), and C is a corrosion allowance (equal to 3.0×10^{-4} m). However, when the D_i is higher than 3 m, t should be at least equal to 0.0127 m to guarantee the support needed to withstand a collapsing pressure. Thus, this was the value considered. The measures and costs of the tanks are presented in Table A 3.

Table A 3- Dimension properties and costs of the tanks considered.

D_i/ m	H/ m	Volume/ m^3	Volume of the liquid (90 % volume)/ m^3	t/ m	W/ kg	$C_{P,updated}$/ €
4.6	5.5	90	81	0.0127	11,294	93,382
6.1	5.5	161	145		16,403	119,218